Surface texture characterization for thin-wall NASA HR-1 Fe–Ni–Cr alloy using laser powder directed energy deposition (LP-DED)

Gradl, P.R.; Cervone, A.; Gill, E.K.A.

DOI
10.1016/j.aime.2022.100084

Publication date
2022

Document Version
Final published version

Published in
Advances in Industrial and Manufacturing Engineering

Advances in Industrial and Manufacturing Engineering 4 (2022) 100084

Contents lists available at ScienceDirect

Advances in Industrial and Manufacturing Engineering

journal homepage: www.sciencedirect.com/journal/advances-in-industrial-and-manufacturing-engineering

Surface texture characterization for thin-wall NASA HR-1 Fe–Ni–Cr alloy using laser powder directed energy deposition (LP-DED)

Paul R. Gradl [a,*], Angelo Cervone [b], Eberhard Gill [b]

[a] Engine Components Development and Technology Branch, NASA Marshall Space Flight Center, Huntsville, AL, 35812, USA
[b] Delft University of Technology, Faculty of Aerospace Engineering, Kluyverweg 1, 2629 HS, Delft, The Netherlands

ARTICLE INFO

Keywords:
Laser powder directed energy deposition
DED
Surface roughness
Thin-wall
Heat exchanger
Fe–Ni–Cr Alloy

ABSTRACT

Additive Manufacturing (AM) offers new design and manufacturing opportunities of thin-wall microchannel heat exchangers for aerospace and industrial applications. Laser Powder Directed Energy Deposition (LP-DED) is an AM process providing large scale manufacturing of thin-wall microchannel heat exchangers. Successful industrialization of the LP-DED process requires critical quantification and understanding of the metallurgical, geometric, and process limitations. Specifically, understanding the as-built surface texture, inclusive of roughness and waviness, is significant due to its effects on the friction factor and pressure drop within a heat exchanger. This experimental study completed a design of experiments (DOE) to determine the critical build parameters that impact surface texture for enclosed thin-wall samples. This study summarizes the characterization work of the LP-DED process for 1 mm enclosed walls with an Fe–Ni–Cr (NASA HR-1) alloy. The LP-DED parameters including laser power, powder feedrate, travel speed, layer height, and rotary atomized powder feedstock were modified in the experiment. An evaluation of the DOE samples and resulting surface texture is provided along with conclusions from these experiments. Results indicate that 3D areal and 2D profile (directional) surface texture is estimated by 2x the powder diameter that becomes captured or partially melted on the trailing edge of the melt pool. The fine powder showed a higher sensitivity to parameter changes but resulted in a higher density material and 23% reduction in roughness. Surface texture was also shown to vary between closed channel shapes (internal) due to ricochets, recirculation, and higher volume of powder available to bond compared to external (outer) surfaces. The understanding of the LP-DED process as-built surface texture is essential to fluid flow applications such as heat exchanges and can modify performance for enhanced heat transfer or can be a detriment to pressure drop.

1. Introduction

Metal additive manufacturing (AM) has demonstrated the ability to fabricate complex geometries with internal features and allow for reduced manufacturing time over traditional manufacturing methods (Blakey-Milner et al., 2021). Laser powder bed fusion (L-PBF) is often the focus of research and hardware applications due the ability to build fine features, but several other metal AM processes are being advanced (Zhang et al., 2017; Kotadia et al., 2021; Liu et al., 2021; Vafadar et al., 2021). These various AM processes each have unique advantages and disadvantages in feature resolution, build volume and deposition rates, metallurgical characteristics, and geometry limitations (Bikas et al., 2019; Sobota et al., 2021). Industrialization of components built using AM require control of the process within a defined set of build parameters (Gradl et al., 2022). The feedstock must also be well-understood to provide results with consistent geometry, uniform microstructure, and meets the requirements of the intended design (Bhuvanesh Kumar and Sathiya, 2021).

One of the common uses of the AM technology is for heat exchangers, where thin-walls with complex flow passages can easily be fabricated (Niknam et al., 2021). Directed energy deposition (DED) and powder bed fusion (PBF) are two relevant AM processes being advanced for this need (DebRoy et al., 2018). Heat exchangers with thin-wall microchannel fabrication using AM have focused almost exclusively on the L-PBF process due to high feature resolution and machine availability (Gradl et al., 2021b). However, the L-PBF process is limited in the overall build volume (Thompson et al., 2015a; Klein et al., 2018; Zhang et al., 2018). This size limitation is based on the (powder filled) build box, typically less than 400 mm in each direction (X, Y, Z), with limited

* Corresponding author.
E-mail address: Paul.R.Gradl@nasa.gov (P.R. Gradl).

https://doi.org/10.1016/j.aime.2022.100084
Received 10 March 2022; Received in revised form 5 May 2022; Accepted 7 May 2022
Available online 12 May 2022

Nomenclature

AM	= Additive Manufacturing
ANOVA	= Analysis of Variance
DOE	= Design of Experiments
HEE	= Hydrogen Environment Embrittlement
L-PBF	= Laser Powder Bed Fusion
LP-DED	= Laser Powder Directed Energy Deposition
NASA HR-1	= Fe–Ni–Cr Hydrogen Resistant superalloy
PSD	= Particle Size Distribution
Pa	= Directional 2D profile average height
Pku	= 2D Profile Kurtosis
Pp	= 2D Profile Peak Height
Psk	= 2D Profile Skewness
Pv	= 2D Profile Valley depth
Pz	= Average Maximum Profile Height
Sa	= Areal Average Surface Roughness
SEM	= Scanning Electron Microscope
Sku	= Areal Kurtosis
Sp	= Areal Max Peak Height
Ssk	= Areal Skewness
Sv	= Areal Max Valley Depth
Sz	= Areal Max Height of Surface
W	= Watts

machines available up to 1 m (Kerstens et al., 2021). One process of interest for larger scale components is laser powder directed energy deposition (LP-DED). LP-DED is a freeform fabrication metal AM process using a laser as the energy source and powder feedstock to melt and fuse metals locally. The laser, which creates the meltpool, is typically central to the integrated deposition head and the powder blown into the melt pool. This can be accomplished with various deposition nozzles with the most common using a coaxial annular nozzle or discrete nozzles, typically 3 or 4, spaced equally around the laser beam (Singh et al., 2020). This entire deposition head is mounted to a motion control system.

The LP-DED process allows large scale fabrication (>2.5 m) using metal powder feedstock, only limited by the robotic or Cartesian gantry system (Lehmann et al., 2021). It is a potential solution offering thin-walls of less than 2 mm for internal features in addition to builds at large scale (Gradl and Protz, 2020). LP-DED offers potential to create large-scale components, such as heat exchangers, with complex geometry, thin-walls, high-density material, controlled microstructure and geometric features (Gradl et al., 2021a). While L-PBF is extensively researched and applied in industry using thin-wall features (Jafari and Wits, 2018; Lin et al., 2019; Kasperovich et al., 2021), there are still gaps in detailed characterization of the LP-DED process. These include surface texture, thin-wall geometry, repeatability, and resulting microstructure (including density) of the material for thin-wall component applications. The melt pool using LP-DED is much larger than the L-PBF process based on the larger spot size (Sow et al., 2020; Jardon et al., 2021). Because of the larger melt pool in LP-DED, forming thin-walls in a single pass bead is required and does not allow for a contour pass, which is a method to improve surface finish using L-PBF (Snyder and Thole, 2020).

The LP-DED process has traditionally been selected for repair operations and to a lesser degree demonstrated for freeform thin-wall additive structures (Ahn, 2021). While the L-PBF process has demonstrated repeatable wall thicknesses down to 0.2 mm (Wang et al., 2017; Gradl et al., 2021b), the LP-DED process does not provide this same resolution. Thin-walls are defined differently by various researchers with most defined as less than 3 mm. Liu and Li demonstrated thin-walls in Steel 24 with LP-DED down to 0.8 mm using a coaxial deposition head and 45–80 μm sized powder (Liu and Li, 2005). Margerit et al. characterized the microstructure of stainless steel 316L using a coaxial deposition head with a 0.2 mm layer thickness and a wall thickness of 0.8 mm (Margerit et al., 2021). Other studies in 316L focused on microstructure and mechanical properties and conducted by various researchers with wall thickness ranging from 0.7 to 2.1 mm (El Cheikh et al., 2012; Balit et al., 2020; Errico et al., 2021; Mianji et al., 2021). The evaluation of superalloy Inconel 718 was also completed with single-track wall thicknesses ranging from 1.3 to 2.5 mm (Bold et al., 2020; Imbrogno et al., 2021; Xu et al., 2021). Other thin-wall research using LP-DED referenced in literature include Hastelloy X with wall thicknesses of 1.7–3.2 mm (Jinoop et al., 2020, 2021), Stainless Steel 410 (Kalami and Urbanic, 2021a), Stainless Steel 304L at 1.2 mm (Arrizubieta et al., 2017), Titanium Ti–6Al–4V (Yan et al., 2020; G. G. Barragan et al., 2021), Gamma Titanium Aluminide at 1.5 mm (Balichakra et al., 2019), Inconel 625 (Kim and Saldana, 2020), CrCoNi (Xue et al., 2021), M4 high speed Steel at 1.7 mm (Jardin et al., 2020), and Al–Mg–Mn-Sc-Zr at 1.6 mm (Zhao et al., 2018). Most of these studies focused on parameter development and the resulting microstructure and mechanical properties. The build specimens were also limited in overall height with many using single-beads and <10 mm overall height. While there is brief mention of surface roughness in some of these studies, the quantified observations are often limited (e.g., contact profilometry, visual inspection) or not provided.

Surface texture (roughness and waviness), often referenced as surface finish, is cited as one of the biggest drawbacks from AM compared to traditional manufacturing technology (Ngo et al., 2018; Rosen and Kim, 2021). The surface texture has an impact on many of the functions related to heat exchangers including fluid flow, thermal management, and mechanical properties. Increased surface texture can adversely affect performance through reduced fatigue and ultimately operational life of a component, increase mechanical friction and wear, increase fluid friction factors related to flow channels resulting in higher pressure drops, and also increase corrosion potential in harsh environments (Stimpson et al., 2016; Hemmasian Ettefagh et al., 2020; Khan et al., 2020; Jones et al., 2021). Surface roughness has been studied in various metal alloys and thin-wall samples using the L-PBF process and applied in various industrial applications (Jamshidinia and Kovacevic, 2015; Fox et al., 2016; Wu et al., 2020). The detailed characterization of surface roughness for thin-wall LP-DED is very limited in literature. Literature suggests that surface roughness and geometric inaccuracies as drawbacks of the LP-DED process and a better understanding of processing parameters is required to control for wider commercial adoption (Azarniya et al., 2019; Errico et al., 2021).

Typical problems associated with LP-DED are all of the surface texture components at various levels; including shape deviation (form), waviness, and roughness. The shape deviation can be caused by residual stresses and resulting distortion that depends on part geometry, alloy, build plate geometry, build parameters, and powder feedstock that all impact the thermal history (Li et al., 2018; Mianji et al., 2021). Surface waviness is often observed in the form of lateral periodic menisci as a result of the stacked deposited build layers, or stair stepping effect (Morville et al., 2012; Zhang et al., 2019). The mechanism identified that causes roughness in LP-DED is residual unmelted and melted powder emanating from the melt pool, ricochets, or excess powder not captured in the melt pool causing powder agglomerations, or adherence to the wall (Jardon et al., 2021). This powder adherence can be a further exacerbated with smaller spot sizes, which are required for thin-walls, due to the low powder efficiency (5–20%) captured in the melt pool (Gharbi et al., 2013; S. A. Wang et al., 2021).

A few studies evaluate surface roughness using the LP-DED process but are limited in the application of thin-walls. The LP-DED system configuration, spot size, and deposition parameters can vary

significantly based on the part geometry and associated wall thickness. Riede et al. completed a study of 316L using a coaxial deposition head and powder sized from 44 to 106 μm and a layer thickness of 0.91 mm and reported an average areal surface roughness, Sa, of 44 μm (Riede et al., 2019). Zhang et al. developed a unique technique for thin-wall LP-DED using a central powder deposition head with surrounding lasers and achieved a surface roughness of 3.2 μm with 75 to 106 μm Fe313 powder and 2.7 mm wall thickness (Zhang et al., 2019). Lu et al. completed a similar study using Fe313 alloy with a central laser beam and 75 to 106 μm powder resulting in 3 μm roughness and a wall thickness of 2.7 mm (Lu et al., 2021).

A study by Mahamood and Akinlabi on LP-DED Ti–6Al–4V suggested increasing laser power using a 2 mm spot size reduced the surface roughness, but was based on a horizontal cladding deposition strategy (Mahamood and Akinlabi, 2014). This increase in power allows for more of the powder to be melted and less residual powder available to adhere to the adjacent surfaces, but the increase in power will impact wall geometry. Kim et al. discuss that an increase in laser power and powder mass flow rate will result in increased wall thickness in addition to providing a consistent bead with less porosity (Kim and Saldana, 2020). A significant increase of laser power solely for thin-wall structures is not a feasible build strategy since this results in uncontrolled geometry. A study by Mazzarisi et al. also confirmed this through deposition of a 1.5 mm wall using Inconel 718 and concluded that 150% increase in laser power caused the melt pool to enlarge and resulted in a 44% increase in wall thickness (Mazzarisi et al., 2020). Jinoop et al. completed an experimental evaluation and concluded that power was the primary contributor to the deposition geometry (width, height, and deposition rate) and powder feed rate and travel speed contributed to a lesser degree (Jinoop et al., 2020). The combination of these parameters is also important since independent adjustments may not always achieve the desired results.

Another study by Mahamood and Akinlabi demonstrated that decrease in the travel speed or increase in shielding gas flow rate could reduce surface roughness, but also focused on a horizontal cladding surface (Mahamood and Akinlabi, 2018). In the thin-wall study by Zhang et al., it was suggested that increasing the travel speed (scan speed) provides a smoother surface due to less dwell time for the excess powder to agglomerate on the surface (Zhang et al., 2019). Alimardani et al. also provided this conclusion to reduce the travel speed to improve surface roughness, but did not provide any quantification of roughness and only visual (Alimardani et al., 2012). Gharbi et al. completed a more detailed study of surface roughness for the LP-DED process on Ti–6Al–4V with wall thicknesses ranging from 1.7 to 3.5 mm (Gharbi et al., 2013). It was observed that the increased travel speed could reduce the waviness in the form of the periodic menisci by a factor of 5, but only had a limited effect on the roughness (26% reduction) with a short interaction distance. Gharbi et al. concluded that the best surface roughness was obtained using higher travel speeds and higher laser power which results in spreading the melt pool.

Motion control parameters such as layer height, injection nozzle stand-off distance, and laser focal plane are referenced in literature with regards to surface roughness. Several articles suggest that reduction in vertical layer height (Z-direction), which can be partially accomplished by the increased travel speed, can improve surface roughness but may not be as efficient as other parameter adjustments (Morville et al., 2012; Gharbi et al., 2013; Balit et al., 2020). The high degree of layering from height changes, resulting in waviness, is commonly observed in literature (El Cheikh et al., 2012; Morville et al., 2012; Imbrogno et al., 2021). Zhu et al. evaluated an approach to change the injection plane to modify the surface roughness, but was focused on the undulations of the top surface and no quantification was provided for the side surface roughness (Zhu et al., 2012). Careri et al. discuss that the stand-off and laser focus distance in LP-DED must be critically controlled to avoid high roughness of the side surfaces and uniformity of the top surface as it relates to post-process machining, but do not quantify this either (Careri et al., 2021).

Powder feedstock is a critical input to the LP-DED process. There are several studies that reference thin-wall deposition using a particle size distributions (PSD) from 45 to 150 μm and a few studies using 15 to 45 μm. Jardon et al. demonstrated 1 mm wall thicknesses using stainless steel 316 L with various PSD, but limited the research to single pass beads on plate and no measurements of surface roughness were provided (Jardon et al., 2021). Based on visual observations, it was suggested that a lower roughness could be achieved using a finer PSD ranging from 15 to 45 μm. A study by Carroll et al. noted that with continued recycling of gas atomized from 50 to 125 μm Waspaloy powder, the surface roughness increased on the sidewalls of 0.6 mm thick samples (Carroll et al., 2006). The article observed that the mean particle size was similar through continued recycling, while flowability increased (reduced Hall Flow values). Ahsan et al. studied the LP-DED process using Ti–6Al–4V gas atomized and the plasma rotating electrode process (PREP) with 45 to 105 μm powders (Ahsan et al., 2011). The mean particle diameter was found to be 94 μm for gas atomized and 72 μm for PREP. The resulting surface roughness was shown to be lower for the PREP powder compared to gas atomized as well as reduced porosity for 3 mm thick samples, although not conclusive if specific to powder size or other contributors. Based on this literature comparing various PSD ranges for LP-DED, further research is merited since the impact to surface texture and roughness was not fully quantified.

Prior literature often suggests that LP-DED requires final machining to achieve desired surface roughness for use in final applications (Gharbi et al., 2013; Dutta et al., 2019). Traditional machining is, however, not feasible for many AM parts, including LP-DED, as complexity increases with internal features such as those for heat exchangers. One of the limitations of the available research is the limited quantification of surface texture relative to as-built thin-walls and enclosed features fabricated using LP-DED. Several publications reference an early study by Li and Ma that evaluated horizontal surface roughness for LP-DED and does not allow roughness to be inferred for vertical surfaces (Li and Ma, 1997), which considers cladding and not vertical thin walls deposited in a single bead. For proper application of surface texture for an industrial application, it must be characterized in the alloy of interest with identical geometry and parameters that are being used for the end part. The surface must be understood beyond an average roughness value (ie. Ra, Sa) since the complexity of the surface can impact the fluid pressure drop, heat transfer, and mechanical fatigue properties. Should post-processing surface enhancements be required to help tune the roughness, the value and dominance of peaks and valleys should be characterized in order to determine the proper material to be removed. Considering observations from the literature, the process parameters (e.g., power, travel speed, layer height, stand-off distance, powder feedrate, shielding gas flowrate), nozzle configuration, and both the powder type and size can be modified to change surface roughness but all potentially at a detriment to geometry.

The results of this research provide an in-depth understanding of surface texture (form, waviness, and roughness) as it relates to 1 mm thick walls using LP-DED processed NASA HR-1 superalloy for heat exchanger applications. The powder feedstock, AM process and associated parameters, geometry, and alloy composition can impact the as-built surface texture and the fluid flow, and the heat transfer performance can vary depending on the surface produced. It is necessary to characterize and understand the sensitivity of the process inputs for each alloy and feedstock of interest so that a designer can properly apply this knowledge for the desired end-use application. NASA HR-1 (Section 2.2) is a Fe–Ni–Cr superalloy used for high pressure hydrogen applications, such as heat exchangers and rocket engine nozzles. The advantage of using NASA HR-1 for these applications is its high conductivity, high fatigue strength, increased yield strength and ductility over other hydrogen-resistant alloys, and excellent hydrogen environment embrittlement (HEE) resistance. Prior literature has shown the advancements made with the NASA HR-1 alloy using LP-DED, but limited

to the metallurgical aspects of the material (Katsarelis et al., 2019; Chen et al., 2021).

Other critical aspects of this research include the detailed characterization of the as-built complex LP-DED surface texture of multi-layer single-bead deposition 1 mm walls using different sizes of rotary atomized NASA HR-1 powder. Prior studies focused on gas atomized powder. This study instead considers as-built inner (enclosed) surfaces and outer (external) surfaces with varying parameters and powder sizes, which were not discussed in prior literature for thin-wall LP-DED. A design of experiments (DOE) was conducted using the LP-DED process parameters and non-contact measurements to characterize the complex as-built surface texture. The as-built surface assumes no post-processing. While the surface texture is critical for design and end-use, the resulting geometry from the build must be balanced with consistency and repeatability of the wall thickness and material density. These were both studied using optical microscopy image analysis. This study provides a quantification for the surface conditions of the LP-DED NASA HR-1 alloy permitting designers to properly account for it and control it for thin-wall applications. This research is relevant for large scale applications (>1 m diameter) where the LP-DED process has advantages for freeform fabrication while still maintaining thin-walls (1–1.2 mm thick). The results presented are relevant to future LP-DED thin-wall components to be used on their as-built surface texture of the walls to reduce post-processing due to costs or the inability to post-process due to complexity.

2. Methodology

The LP-DED process uses a laser beam to create a melt pool and metal powder is injected into this pool using an inert carrier gas through a deposition head. As the deposition head traverses an area that was deposited the material cools and then solidifies creating the bead. The deposition head is attached to a motion control system, such as a multi-axis robotic arm or Cartesian coordinate gantry system. The Cartesian coordinate gantry system is preferred and was used in this study allowing for better accuracy and repeatability, which is critical for single-width bead wall thickness. After a single layer is built for the samples or part, additional layers are deposited until the final part is created. LP-DED also has the advantage of using multiple axis for complex geometries and is not limited to only 3-axes.

The samples created for this study were single-width bead racetracks with 75 mm length, 25 mm in height, and 1 mm wall thickness (adjacent walls spaced 25 mm apart). These were deposited as a racetrack as opposed to a freestanding wall to provide geometric stability and eliminate any distortion. Each sample was deposited according to the parameters established for the DOE and then measured using non-contact microscopic imaging to evaluate texture and roughness. Further characterization of the wall thickness and porosity was evaluated using microscopic and scanning electron microscope (SEM) imaging.

The LP-DED system has several subsystems that include the powder injection and purge gas flow system, the laser power supply and optics, and the motion control. Each of these subsystems must work congruently to provide the desired bead, resulting geometry, and material characteristics. These subsystems use support hardware and input parameters that can be adjusted to affect the material characteristics, including surface roughness. The laser and optical system includes many of the laser parameters and optical hardware that derive the beam delivery including the power, spot size, focus position, profile of beam, type of laser, and laser operational mode (such as continuous or pulsed). The powder injection system includes systems and inputs such as the powder feedrate, type of carrier gas, core shielding gas and/or secondary gas flow (mass flow rate and gas type), and the powder nozzle design (annular or multi-nozzle). The motion control system manipulates the movement parameter for the deposition head that includes the travel speed, sets layer height, standoff distance, angle of the head, and hatching (or step-over). While these parameters are fundamental to the basic build geometry, other factors may be more specific to component build geometry, such as spacing between features, build plate configuration, and toolpath build strategy. The major subsystems and parameters for LP-DED are shown in Fig. 1.

The primary parameters that are critical to the LP-DED process include laser power, travel speed (also called feedrate or scan speed), powder feedrate, laser spot size, hatching (also called stepover spacing or track overlap), and layer height (or layer thickness) (A. S. Wang et al., 2021). These parameters and some of the other process inputs shown in Fig. 2 determine the melt pool and resulting geometry. The melt pool and powder carrier gas derive the general surface roughness (Shah et al., 2010). An unstable melt pool can cause spatter, porosity, or irregular beads and increase occurrences of unmelted or partially-melted powder adhering to the surface.

2.1. LP-DED experiment parameters

This study specifically focused on five key input parameters and impacts to the resultant surface texture. The down selected parameters include the laser power, travel speed, layer height, flow rate of powder, and powder size and are highlighted in Fig. 2. Several parameters were fixed based on the geometry desired and also system configuration. The spot size selected was determined by the desired wall thickness, in addition to the type, mode and subsequent profile of the laser were all fixed. The standoff was also considered but is accurately controlled in the motion system with monitoring. The angle of the head is fixed normal to the surface. Other parameters such as angle of the head, hatching, and build strategy were not applicable since the experiment involved single bead width thin-wall deposition.

A total of 35 samples were fabricated on an RPM Innovations (RPMI) 557 machine with a 3-nozzle Argon-carrier gas powder injection and Argon central purge deposition head. This was a gantry-type system, and the build box was fully inert with Argon to reduce oxidation. The laser used was an infrared (IR) 1064 nm continuous wave with Gaussian profile. All samples were single bead width deposition tracks in the Z-direction. The sample tracks were fabricated on a 13 mm thick mild steel build plate.

The baseline parameters were established through initial experimentation to demonstrate a low porosity NASA HR-1 build that would meet geometric requirements as well as optimal deposition time. The variation in parameters for this experiment were selected to be 5% from nominal for power, travel speed, powder feedrate, and 10% for layer height. These were selected to ensure that all build samples would be successful to full height for data analysis in addition to meeting wall thickness range of 1–1.2 mm. While parameters could be varied further, this would result in incomplete or failed samples and data could not be collected. Other studies suggest that a higher increase in laser power of 25% or more could improve surface roughness (Gharbi et al., 2013). However, core material microstructure and desired geometry must also be considered. With increased power for thin-wall LP-DED, the melt pool increases resulting in thicker walls, increased size and quantity of the columnar grains, and results in a more porous structure (Kim and Saldana, 2020). Additionally, the NASA HR-1 could be adversely impacted with increased laser power through vaporizing of strengthening elements or segregation of these elements, both resulting in a poor material microstructure and properties (Chen et al., 2021).

Each sample was deposited using a racetrack configuration (flat walls and 180° radii) to provide dimensional stability and allow for surface texture (waviness and roughness) to be measured on both the inner (internal to racetrack) and outer (external) surfaces (Fig. 3). The samples were 76 mm in length (Y-direction), 25 mm in height (Z-direction) and opposing walls spaced 25 mm apart (X-direction). The area selected for surface measurements was 43 mm in width and 16 mm in height. The samples were sectioned from the build plate via bandsaw and were cleaned in Isopropyl alcohol to remove any excess machine oil.

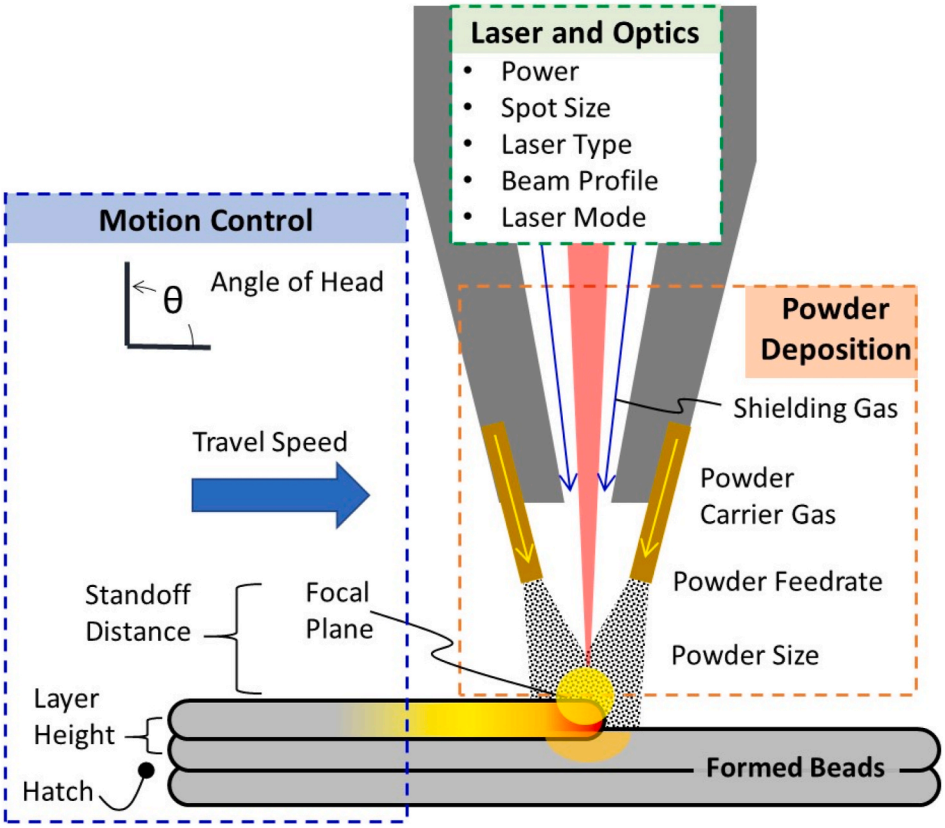

Fig. 1. Overview of LP-DED process parameters and inputs.

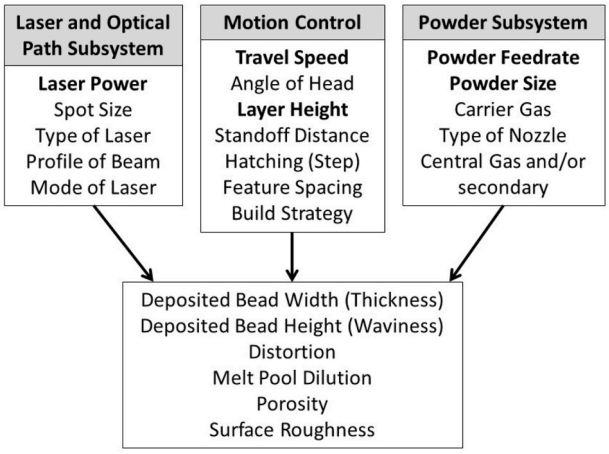

Fig. 2. LP-DED parameter inputs that can impact surface texture and the deposited bead geometry. The highlighted parameters were varied in this study.

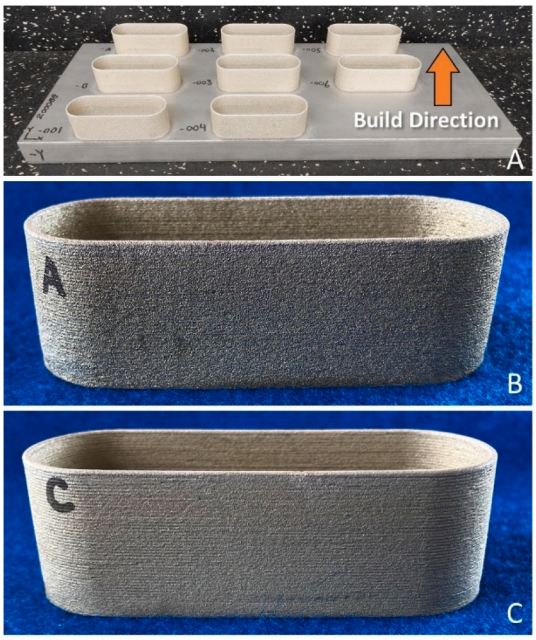

Fig. 3. Fabricated experimental select samples. A) Deposited samples on build plate, B) Sample A (Run 32) with nominal parameters using 45 to 105 μm powder, C) Sample C (Run 34) with nominal parameters using 10 to 45 μm powder.

No mechanical cleaning was used to preserve the surface. The samples are referenced by a unique indicator (1–35), however the last four samples in series (32–35) were labeled as A-D to indicate nominal parameters. A built plate with samples (1 through 6, 32, 33) is shown in Fig. 3A. The typical surface from a coarse powder sample (45 to 105 μm) is shown in Fig. 3B and fine powder (10 to 45 μm) in Fig. 3C.

2.2. NASA HR-1 material

The NASA HR-1 alloy was selected for this study due to the importance of this alloy for use in hydrogen based heat exchanger applications (Katsarelis et al., 2019). The NASA HR-1 alloy was developed at NASA Marshall Space Flight Center in the late 1990's as a hydrogen environment resistant (ie. "HR") superalloy for use in high temperature and high pressure hydrogen applications (Chen and Mitchell, 2005). NASA HR-1 is a Fe–Ni–Cr Superalloy that provides high strength and high ductility

in these harsh environments and originally derived from JBK-75. The alloy has been demonstrated in several applications focused on liquid rocket nozzles and high temperature hydrogen environment heat exchangers (Gradl et al., 2021a). While other alloys exist that could meet these general requirements, such as A-286, JBK-75, and the 300 series stainless steel (304, 310, 316), they can be limited in strength for such heat exchanger applications (Gradl and Protz, 2020).

Two powder lots (HRA9 and HRA4) of rotary atomized NASA HR-1 from Homogenized Metals Inc. (HMI) were used for the sample deposition in a fine cut (10 to 45 μm) and coarse cut (45 to 105 μm). The powder chemistry was within nominal ranges including any trace elements that were measured (C, Mn, Si, P, S, B) as seen in Table 1. Chemistry was measured using Inductively Coupled Plasma (ICP) at HMI.

The rotary atomized powder was characterized using a Microtrac (Version 10.1.0.6) and imaged using a Hitachi S3000H Scanning Electron Microscope (SEM) to evaluate the general morphology. The fine and coarse cut powder SEM images can be seen in Fig. 4. The Microtrac calculated the peak distribution of the powder at 70 μm for the coarse powder (45 to 105 μm). The SEM showed mostly spherical shape with a few oblong ellipsoidal particles and some traces of satellites for the coarse powder. Oblong particles can cause issues with flowability or clog the nozzle during deposition. The fine powder (10 to 45 μm) showed a peak at 34 μm from the Microtrac characterization. While a majority of the finer powder is spherical observed in the SEM, the oblong shaped morphology is also observed along with several sphere and satellites and granular particles.

2.3. Design of experiment (DOE) samples

A DOE was developed to understand the relationships between the input process parameters, powder feedstock in two different PSDs, as well as significant interactions of the parameters on the resulting surface texture and roughness. A split design grouped by powder size was selected for the DOE because of the difficulty of powder changes. This avoided changing powder every run, which was not feasible for the experiment. A total of 35 runs (Runs 1–35) were completed at varying parameters including four distinct runs (two with each powder size) at the predetermined optimal set of parameters from prior development work on this alloy. The predetermined optimal set of parameters was laser power = 350 W, powder feedrate = 23 g/s, travel speed = 762 mm/s, and layer height = 0.254 mm. The summary of parameters used for this study is shown in Table 2.

The DOE was analyzed using analysis of variance (ANOVA) to determine the significance and extent of influence for the LP-DED process parameters that impact surface texture (Montgomery, 2019). The overall model and influence of the individual factors and interactions were considered significant if the probability value (p-value) was less than the set significance level ($\alpha = 0.05$). This analysis was conducted using DesignExpert software. The final model that best fit the data was a two-factor interaction (2FI), with several terms eliminated that were not significant. Other models were evaluated including quadratic but did not provide any significance.

Table 1
Chemistry for NASA HR-1 powder used in this study (Wt. %).

Element	Powder Lot		Nominal Chemistry
	HRA9	HRA4	Ref (Katsarelis et al., 2019)
PSD	10 to 45 μm	45 to 105 μm	
Fe	41.24	41.78	Bal
Ni	33.91	33.71	33.7–34.3
Cr	14.66	14.49	14.3–14.9
Co	3.79	3.75	3.6–4.0
Mo	1.83	1.82	1.6–2.0
Ti	2.41	2.31	2.2–2.6
Al	0.243	0.24	0.23–0.27
V	0.302	0.30	0.28–0.32
W	1.60	1.59	1.4–1.8

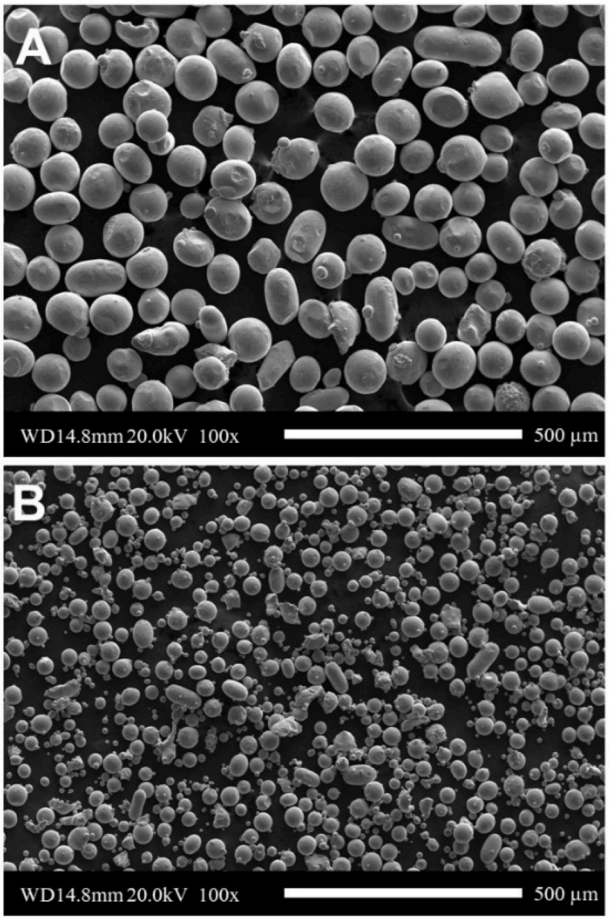

Fig. 4. SEM Images of the NASA HR-1 Powder. A) Coarse cut 45 to 105 μm powder and B) Fine cut 10 to 45 μm powder. Note: both images are at the same magnification (100X).

2.4. Roughness measurements and microscopy

Each sample was then measured using a non-contact Keyence VR-5200 patterned light projection profilometer with three telecentric lenses at 80x magnification and image stitching with an overlap of 20%. The samples were first measured on the outer surface, then sectioned inside the radii and measurements were completed on the inner surface. A surface form correction was used on the entire area to remove the tilt and any curvature, and a reference plane was then established. No filtering was used in the analysis of the surface topography data since the entire surface is of interest for potential thin-wall applications. All measurements were completed and reported according to ASME B46.1 (American Society of Mechanical Engineers (ASME), 2019). The surface scanning covered an area of 43 mm by 16 mm and areal measurements for average roughness (*Sa),* max *height of surface (Sz),* max *peak height (Sp),* max *valley depth (Sv), skewness (Ssk), kurtosis (Sku*) were determined from this region. Waviness was obtained in the horizontal and vertical directions with a high-pass filter (λc) of 0.25 mm and low-pass (λs) of 0. The focus of this study was on the sidewall vertical surface roughness, which is in the direction of flow for heat exchanger applications. The measurement uncertainty was obtained by repeating measurements on a single sample for each fine and coarse powder PSD samples. A 99% confidence interval for measurement uncertainty is calculated and presented in the data plots.

In addition to areal surface analysis, five vertical lines and three

Table 2
Selected Parameters and Powder for DOE runs.

Sample ID	Powder Change	Laser Power	Powder Feedrate	Travel Speed	Layer Height	Powder Size
		W	grams/sec	mm/min	mm	µm
1	1	333	23.0	724	0.254	45–105
2	1	350	21.9	724	0.279	45–105
3	1	333	24.2	762	0.229	45–105
4	1	350	24.2	762	0.254	45–105
5	1	333	21.9	800	0.229	45–105
6	1	368	23.0	762	0.254	45–105
7	2	333	21.9	762	0.254	45–105
8	2	368	24.2	800	0.229	45–105
9	2	350	23.0	724	0.229	45–105
10	2	350	21.9	762	0.254	45–105
11	2	368	23.0	724	0.279	45–105
12	2	333	24.2	800	0.279	45–105
13	3	350	23.0	762	0.254	10–45
14	3	350	23.0	762	0.279	10–45
15	3	368	24.2	724	0.229	10–45
16	3	368	21.9	800	0.229	10–45
17	3	333	24.2	800	0.229	10–45
18	3	333	21.9	800	0.279	10–45
19	3	333	21.9	724	0.229	10–45
20	4	350	23.0	800	0.254	45–105
21	4	368	24.2	762	0.279	45–105
22	4	368	21.9	724	0.229	45–105
23	4	350	24.2	724	0.254	45–105
24	4	333	23.0	762	0.279	45–105
25	4	368	21.9	800	0.279	45–105
26	5	333	23.0	800	0.254	10–45
27	5	368	21.9	724	0.279	10–45
28	5	350	23.0	762	0.254	10–45
29	5	333	24.2	724	0.279	10–45
30	5	368	24.2	800	0.279	10–45
31	5	350	23.0	762	0.229	10–45
32	1	350	23.0	762	0.254	45–105
33	1	350	23.0	762	0.254	45–105
34	5	350	23.0	762	0.254	10–45
35	5	350	23.0	762	0.254	10–45

horizontal line profiles were obtained from the surface areal profile. The vertical direction corresponds to the build direction and also flow direction in heat exchangers fabricated with LP-DED. The 2D profile directional line texture parameters analyzed were average profile height (*Pa), average maximum profile height (Pz), reduced peak height (Pp), reduced valley depth (Pv), skewness (Psk), and kurtosis (Pku*). The profile texture measurements (Pa, Pz, Pp, Pv, Psk, Pku) were used for this experiment which is inclusive of waviness and roughness that could impact the application for flow in heat exchangers. This is synonymous with the traditional Ra (average roughness) but are not filtered for waviness. The line profile data is important to the end application, and directionality should be considered for specific applications (Kalami and Urbanic, 2021b), such as fluid flow, and included as an outcome of this study. The 2D directional profile measurements were equally spaced across the region of interest in the vertical and horizontal directions. The regions of interest for the areal surface roughness and directional texture measurements are shown in Fig. 5. For data reporting, the five vertical texture measurements were averaged, as well as the three horizontal measurements averaged, to provide a single value. All measurements were repeated for the inner and outer surfaces for each sample.

Following the texture measurements, SEM imaging was completed on a Hitachi S3000H for select samples on the inner and outer surfaces within the central region of the sample. The samples were then sectioned and mounted to evaluate porosity and microstructure. The micrographs were imaged using a Keyence VHX digital microscope. The samples were prepared per ASTM E3 using a Presi automatic polisher. The samples were prepared to evaluate porosity were polished using 0.05-µm colloidal silica, but not etched. This allowed for image characterization of the potential defects independent of the visible grain structure. Select samples were etched using etchant #13 (10% Oxalic Acid, Electrolytic) to determine the deposition melt patterns and general grain structure.

The porosity was measured on the polished samples using ImageJ software (Version 1.53e). The image was adjusted to 8-bit to allow for differentiation between pores and other stains or burns that can occur from polishing. The entire area of the sample was then selected, and the areas of porosity quantified; any edge effects were eliminated to minimize error. The samples thickness was measured using ImageJ at five transverse locations and then averaged to provide a single value.

3. Experimental results

3.1. Visual and SEM

All samples from the LP-DED process were built successfully (no failures, no process stops, no issues noted) to the nominal dimensions. The samples were removed from the build plates and evaluated in the as-built condition (i.e., no stress relief or subsequent heat treatments; no

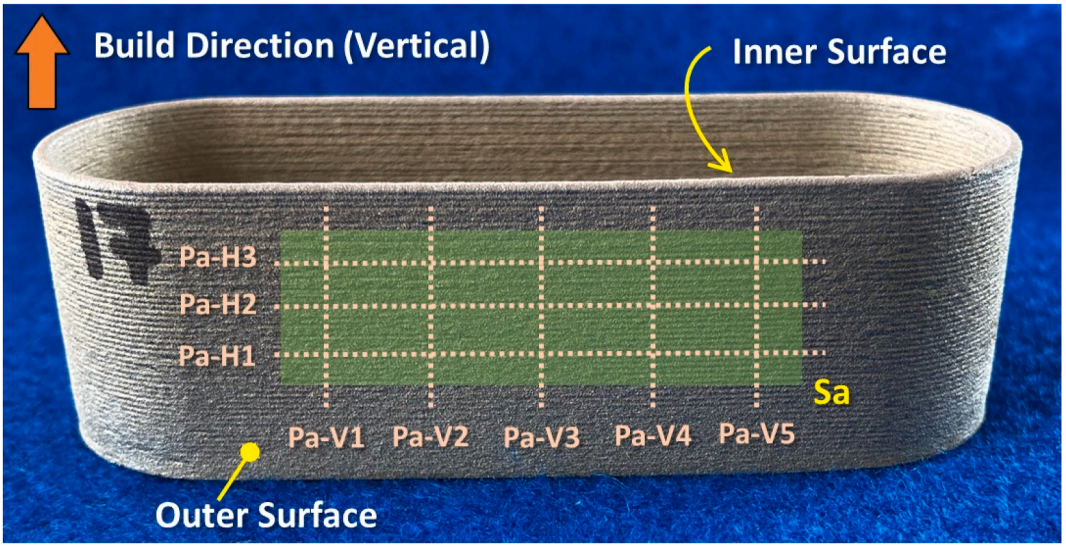

Fig. 5. Nomenclature and measurement locations for areal and directional profile line texture measurements. The build direction also corresponds to the flow direction for heat exchanger applications.

surface modifications). The coarse powder samples appeared to have a higher degree of texturing across the surface, and the fine powder samples emerged smoother from visual inspections. The SEM images show the surface roughness being impacted by the powder size, as seen in Fig. 6. The coarse powder samples have a random powder scattering across the surface (Fig. 6A) of partially melted and loosely adhered powder (Fig. 6B). Several powder particles can be seen barely protruding from the surface encapsulated by the solidified surrounding material, while the partially melted and solidified material forming a radius with the underside of the particles. The fine powder samples (Fig. 6C and D) show a higher number of particles adhered, covering adhered covering almost the entire surface. There is minor visual evidence of the macro waviness observed in Fig. 6C, potentially from layer height. There are many instances of fully melted and partially melted fine particles similar to the coarse powder. The diameter of the particles measured normal to the surface on the SEM images match the PSD of the powder sizes used for respective samples.

3.2. Microstructure

Representative sectioned and etched samples for coarse and fine powder are shown in Fig. 7. The sample with coarse powder (Fig. 7A, B, C) displays the particles adhered to the surface with solidified material forming a tangential radius between. In most instances, the melted and solidified material extends about 50% of the width of the particle, forming the roughness on the surface assuming powder particles protrusions are defined as roughness and the layering is defined as waviness, as suggested by Diaz (2019). There are a few instances observed with subsurface particles that are not fully melted into the surrounding material and shown to be a maximum of 2x the diameter of the powder PSD. The unmelted coarse particles extend about 150 μm subsurface measured normal from the surface. The fine powder sample (Fig. 7D, E, F) shows a higher number of instances and higher density of unmelted powder across the surface and subsurface. There are multiple layers of unmelted or partially melted fine powder observed subsurface with solidified material between the particles. The unmelted particles extend about 100 μm into the subsurface when measured normal from the external surface.

The melt pools are clearly visible in the etched samples. The microstructure is characteristic of the LP-DED process with epitaxial dendrite grain growth that traverse across melt pools (Bian et al., 2015; Shamsaei et al., 2015; Gamon et al., 2021). The dendrite arm growth is random, but also shows a tendency to solidify from the outer surface of the melt pool towards the center. Small grains are observed on the external surface of the samples due to the rapid cooling (Thompson et al., 2015b). The rapid cooling of the exterior surfaces trap excess powder with solid material, surrounding these loose particles.

3.3. Areal measurements

The areal roughness measurements (Sa, Sz, Sku, and Ssk) for all of the specimens are summarized in Fig. 8. Sa is the typical areal parameter used to quantify roughness of surfaces but does not capture the complexity and discriminate between peaks and valleys. The Sz, Sp, Sv, Sku, and Ssk parameters define the magnitude of the peaks and values that can be used in fluid flow evaluations for heat exchangers or material removal estimates for post-processing operations (e.g. machining or polishing). The DOE samples were each built with a varying set of

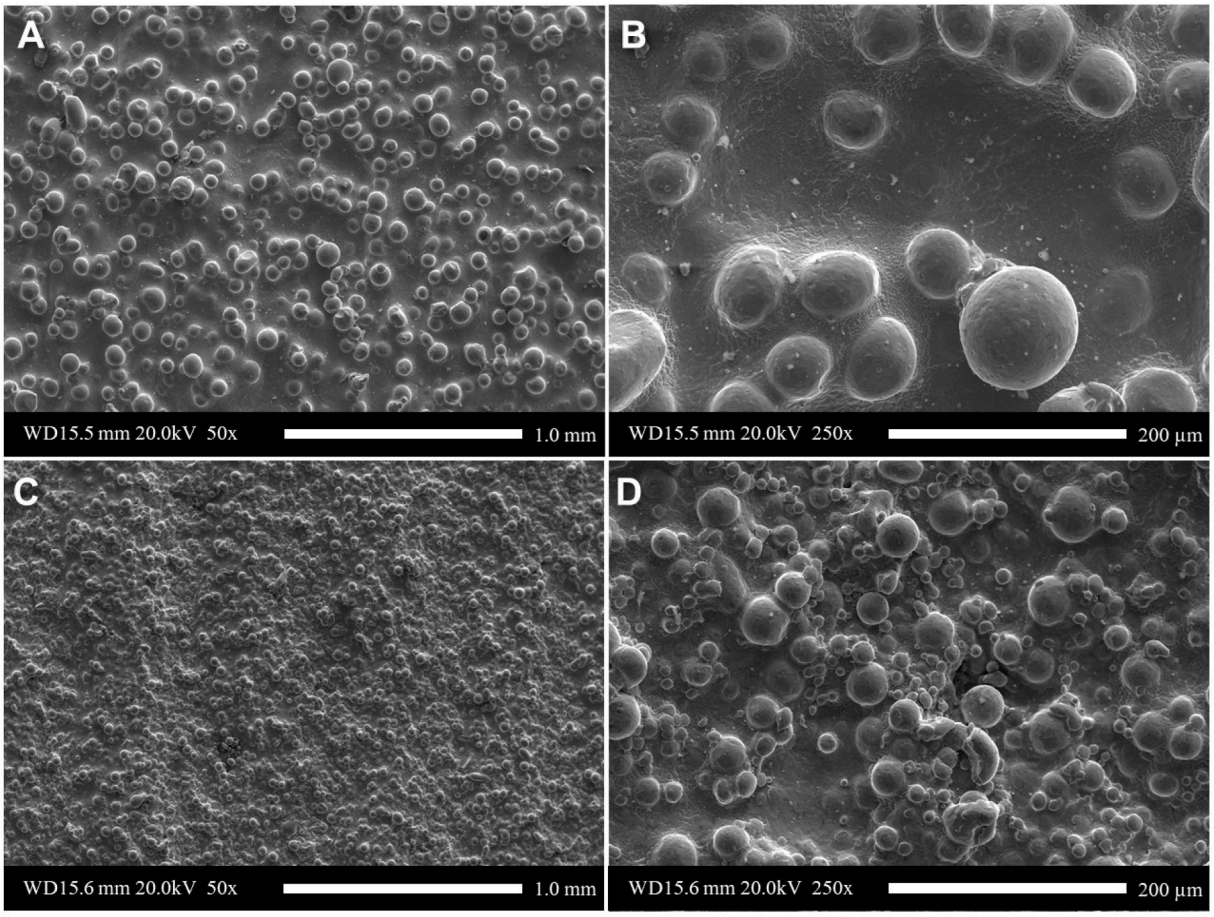

Fig. 6. SEM images of select samples. A) Sample 32 inner surface with coarse powder at 50x, B) Sample 32 inner surface with coarse powder at 250x, C) Sample 34 inner surface with fine powder at 50x, D) Sample 34 inner surface with fine powder at 250x.

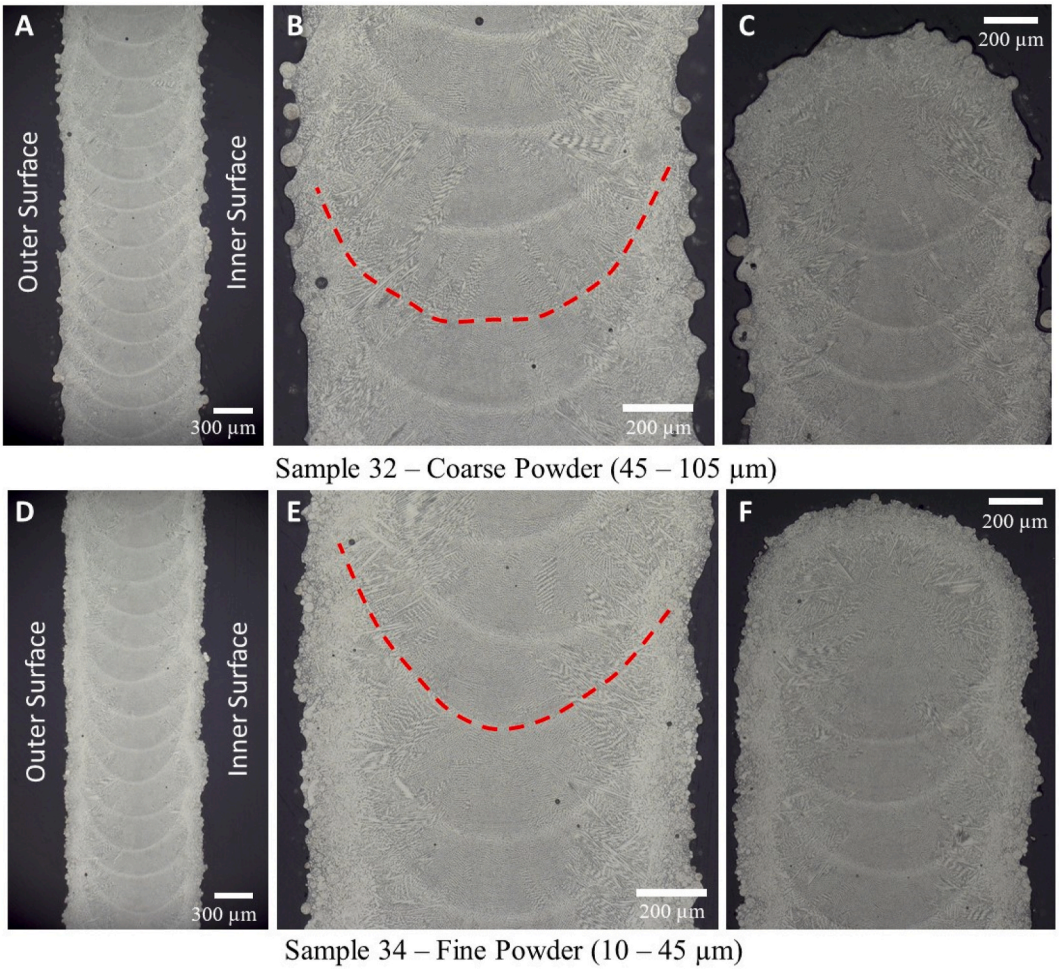

Fig. 7. Sectioned and etched samples with inner and outer surfaces. A, B, C) Sample 32 using coarse powder, D, E, F) Sample 34 using fine powder.

parameters and identified by sample number on the X-axis of plots, which is synonymous with run number (Table 2). The average areal roughness (arithmetic mean deviation), Sa, in Fig. 8A clearly shows the fine powder is lower compared to the coarse powder in almost all samples, which is consistent with prior observations (Kong et al., 2007; Jardon et al., 2021; Kladovasilakis et al., 2021). The dotted lines in Fig. 8A is to pair the samples inner and outer wall data points for readability.

Another trend observed is the difference between the inner and outer surface with the inner surface showing higher roughness in almost all instances for both fine and coarse powders. This is due to ricochets, recirculation, and higher volume of powder available on the internal volume of the racetrack sample to bond with the trailing edge of the melt pool during solidification. There is a high volume of powder available due to the low efficiency (<10%) with thin-wall depositions such as this. The Sa for the coarse powder shows a tight grouping of data independent of the changes in parameters, where the fine powder has more variation. The fine powder shows higher sensitivity in changes to build parameters. The areal roughness, Sa, for the fine powder showed a downward trend as a function of energy density. The coarse powder was stable as a function of the energy density. From the dataset, sample 30 appears to be a clear outlier, which is partially impacted from the waviness from the layering. This was the only sample where all build parameters were set to the higher range (power = 368 W; powder feedrate = 24.2 g/s; travel speed = 800 mm/s; layer height = 0.279 mm).

The amplitude parameters for Kurtosis (Sku) and skewness (Ssk) were evaluated and shown in Fig. 8C and D. The high Sku (>3.0) indicates that all samples have a high degree of peaks and valleys across the surface. The coarse and fine powder samples show minor variation within the groups and indicates the predominance of peaks across the surface (based on Ssk). Most of the coarse samples are dominated by peaks. Ssk trends downward as energy density increases independent of powder PSD, but only for the inner surface.

3.4. Directional profile measurements

The 2D directional profile texture results are similar to the areal parameters and shown in Fig. 9. These parameters were measured in the vertical direction at a length of 16 mm. The trends are very similar with the coarse powder PSD showing higher values than the fine powder PSD. The dotted lines in Fig. 9A pairs the samples together for readability. For a majority of samples the average profile height of the inner surface (Pa) has a higher texture than the outer surface, although some are reverse compared to Sa such as samples 1, 8, 25. Pa is a localized measurement and any excess powder, particularly with the coarse PSD, in a localized area could change the values. The largest disparity is 9% (sample 8) and with the measurement uncertainty cannot be shown statistically different.

The average maximum profile height for the vertical (Pz) measurement is grouped tighter for the coarse powder and similar for the fine powder. The high measurement uncertainty for the coarse powder represents the random coarse particle adherence causing larger peaks and valleys. The Pz of the inner surface is generally higher than the outer surface, but variations can be attributed to location dependency. The Pku is similar to the Sku and the surface is dominated by a high degree of peaks and valleys for all coarse samples and to a lesser degree the outer

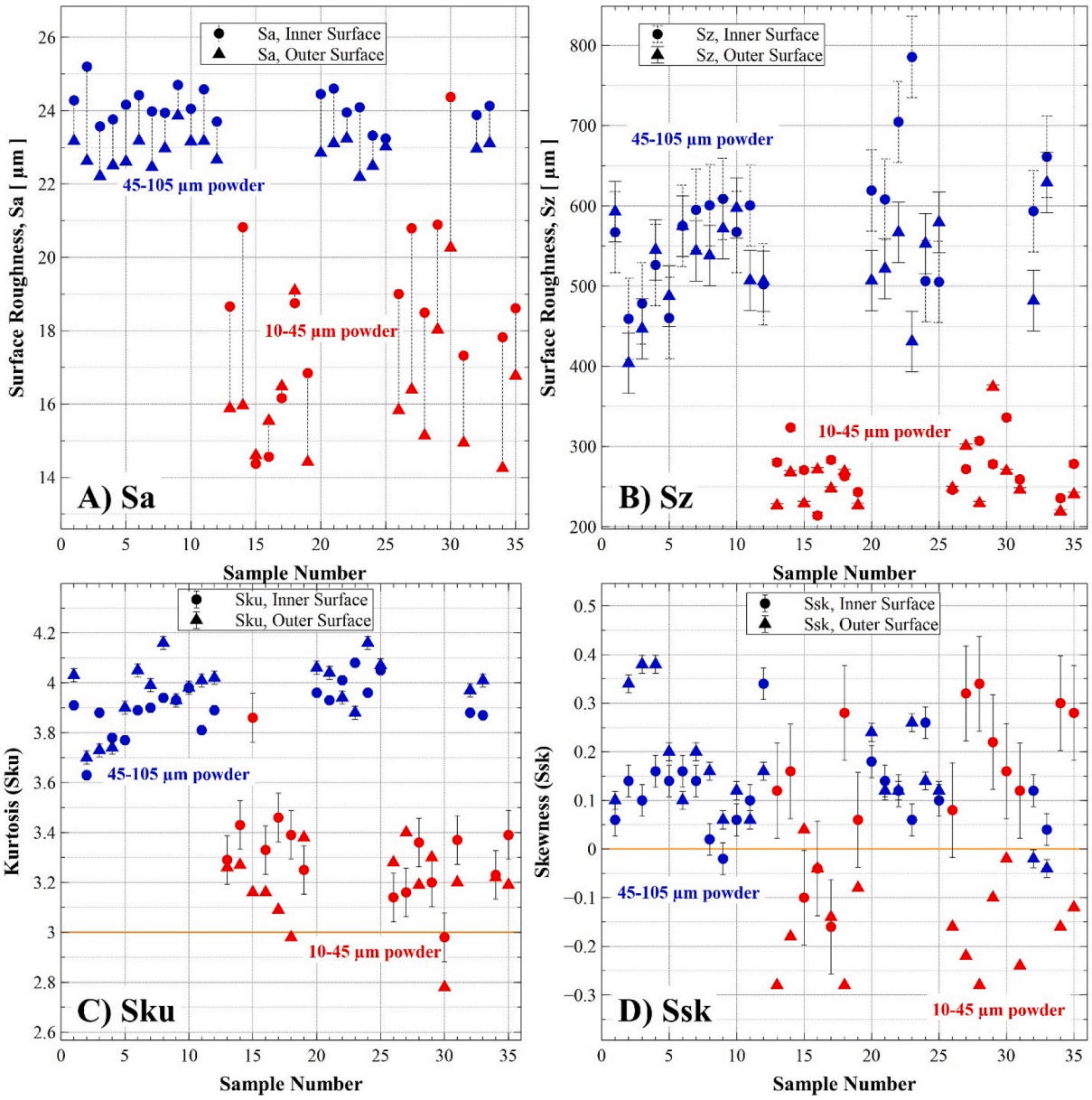

Fig. 8. Areal texture measurements for all samples. A) Average area roughness [Sa], B) Maximum height of surface [Sz], C) Kurtosis [Sku], D) Skewness [Ssk].

surface fine powder samples. The peaks (Pp) and valleys (Pv) for the inner surface is observed in Fig. 9A and D for the outer surface. The Psk indicates that peaks are still dominate on most of the samples. The 2D profile values, specifically Pa, Pz, Pp, Pv, Pku, Psk are also important to report since fluid flow in heat exchangers is directional and may be used in flow performance evaluations such as friction factors.

3.5. Waviness

Typical LP-DED samples have shown layering undulations from the dilution of vertical melt pools created on the sidewalls forming waviness (Gharbi et al., 2013; Tan et al., 2020). In prior literature this layering is apparent in the cross-section of the deposited samples (Morville et al., 2012; Imbrogno et al., 2021). Within this current study, the layering and undulations are not visible in the sectioned samples. The vertical waviness is shown in Fig. 10 and shown to be more preferential to the inner surface. The dotted lines are provided to enhance pairing of samples for readability. The coarse samples are all within 15% of the average with the exception of sample 12. The coarse samples did not show any statistical trends in waviness compared to layer height, while the fine samples indicated increased waviness with increased layer height. The finer powder PSD samples have a higher degree of variation showing higher sensitivity to the process parameters and resulting melt pool geometry (Kladovasilakis et al., 2021). Sample 30 has higher waviness compared to other samples with all the deposition parameters set at the highest values. The increased layer height in addition to higher power and increased powder feedrate causes the melt pool to spread, resulting in higher waviness.

3.6. DOE results

The DOE data were analyzed using ANOVA with the process parameters as the factors and the surface roughness (Sa) data as the response. The final model that best fit the data was a two-factor interaction (2FI), with several terms eliminated that were not significant. The results from the ANOVA of the inner surface roughness are provided in Table 3 with an overall R^2 fit of 97.8% for the selected factors. The results show that powder size is the major contributor at 71% of the

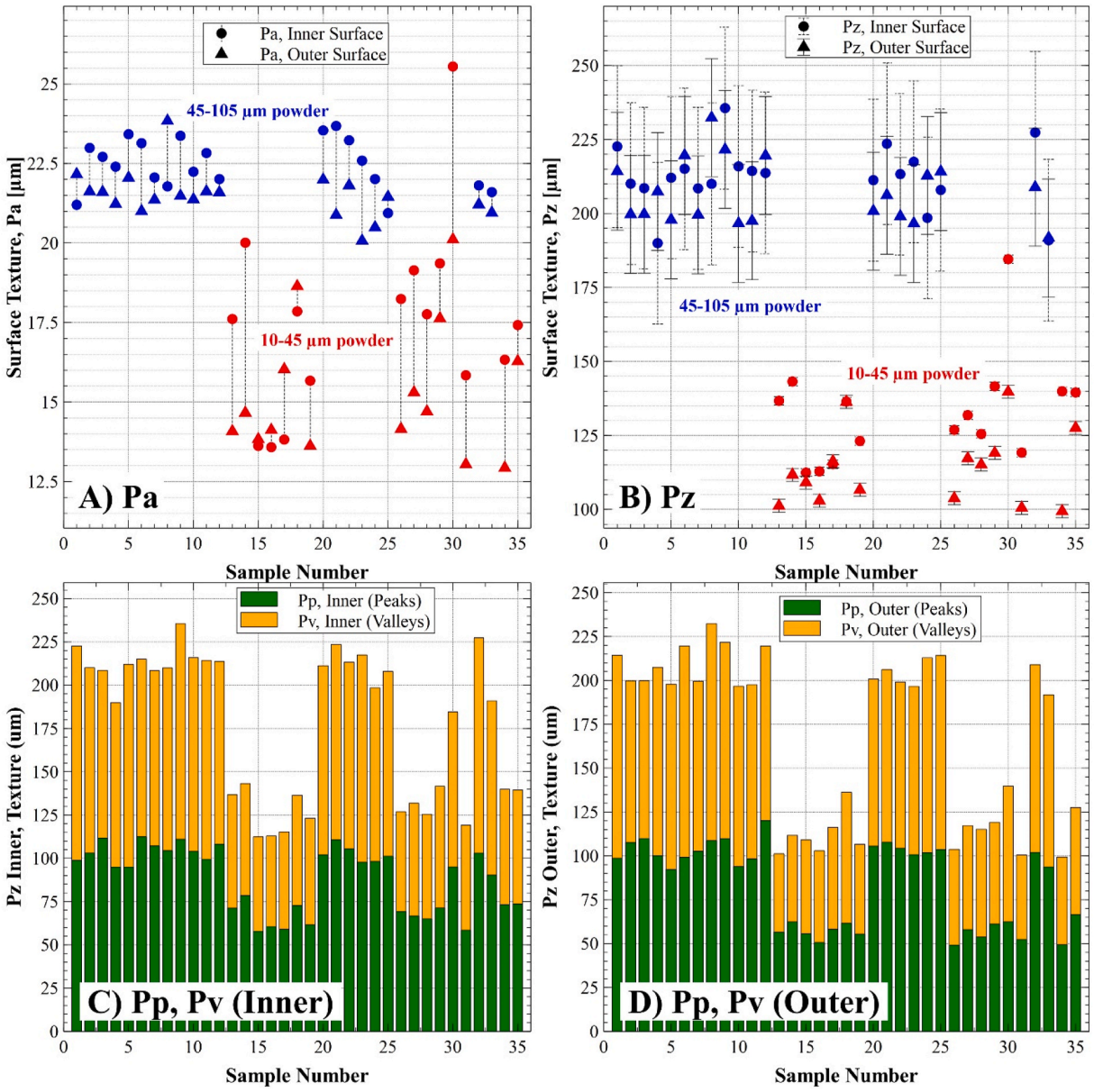

Fig. 9. Directional vertical texture per sample. A) Average profile height [Pa], B) Average maximum profile height [Pz], C) Measured peaks [Pp] and valleys [Pv] for inner surface, D) Measured peaks [Pp] and valleys [Pv] for inner surface.

overall model, as observed in the average areal roughness data. The layer height is also a contributor and the interaction between layer height and powder size at 10% each. Other interactions of the parameters were significant in the model, but not major contributors to the texture or roughness. Prior studies by Gharbi et al. and also Ahsan showed a correlation between the roughness and the energy density that as energy density increased the roughness also increased (Ahsan, 2011; Gharbi et al., 2013). A major difference in those studies compared to this was a significant variation in power, where this study focused on a 5% difference. This study was also focused on maintaining a consistent and thin wall, so significant increases in energy density would increase the melt pool diameter and subsequent wall thickness.

3.7. Porosity

The porosity of each sample compared to the Sa values is shown in Fig. 11. All fine powder samples have a measured porosity of less than 0.061%, average of 0.031% ± 0.01% and low value of 0.014% (range of 0.047%) consistent among all fine PSD samples. The coarse powder samples had a much wider distribution of porosity and ranged from 0.052% up to 0.307% and average of 0.13% ± 0.07%.

3.8. Sample wall thickness

Thickness variation was evaluated through direct measurements of the cross sectioned samples. The results of the overall thicknesses along with powder size and laser power are shown in Fig. 12. An ANOVA was also established to evaluate the build parameters impacting thickness. While the model showed several factors were significant for several factors and interactions, the R^2 fit was only 82.7%. A major contributor to the thickness model was laser power (25.3%) and travel speed (22.3%). Layer height had a small contribution (5.5%) as well as powder size (4.6%) and interactions of the parameters (16.6%). Fig. 12 indicates some visual correlation of thickness to laser power, although all parameters are being adjusted simultaneously.

The process hardware and setup for building the desired wall

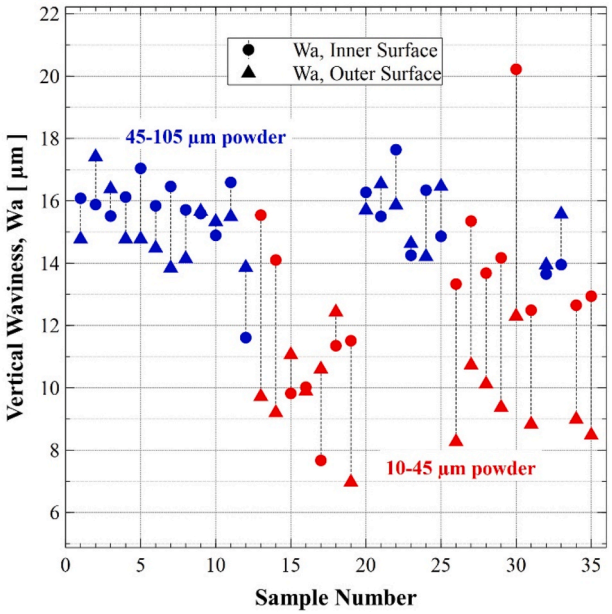

Fig. 10. Vertical waviness for inner and outer surfaces.

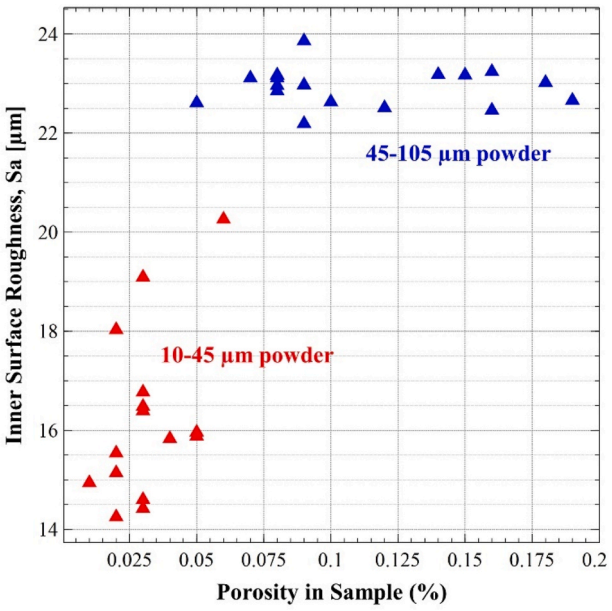

Fig. 11. Porosity measurements in samples compared to inner average areal surface roughness (Sa).

Table 3
ANOVA for average inner surface roughness (Sa).

Source	Sum of Squares	DoF	Mean	F-value	p-value
Model	359.2	11	32.7	91.3	<0.0001
A-Laser Power	0.1	1	0.1	0.2	0.6432
B-Powder Feedrate	1.2	1	1.2	3.3	0.0804
C-Travel Speed	0.0	1	0.0	0.1	0.7212
D-Layer Height	35.3	1	35.3	98.8	<0.0001
E-Powder Size	259.6	1	259.6	725.9	<0.0001
A*C	1.2	1	1.2	3.4	0.0782
A*D	4.7	1	4.7	13.1	0.0014
B*C	5.7	1	5.7	15.8	0.0006
B*D	2.8	1	2.8	7.7	0.0106
B*E	2.4	1	2.4	6.7	0.0163
D*E	37.0	1	37.0	103.6	<0.0001
Residual	8.2	23	0.4		
Lack of Fit	7.7	19	0.4	3.4	0.1236
Pure Error	0.5	4	0.1		
Cor Total	367.5	34			

thickness can have an impact on the final surface roughness. The melt pool resulting in 1 mm wall thickness results in a lower catchment efficiency of 5–20% (Gharbi et al., 2013). The powder that is captured in the melt pool is often drawn to the center due to Marangoni flow (Singh et al., 2020). Particles that are not fully molten can be expelled from the melt pool and adhere to the sidewalls or trailing edge (Kalami and Urbanic, 2021b). The residual powder (80–95%) not captured is then available to bond to the trailing edge of the melt pool in the outmost surface and then rapidly cooled (Zekovic et al., 2007; Prasad et al., 2019). This is further exasperated in thin-walls due to low thermal mass and accelerated cooling rate. For practical applications of the LP-DED process, the geometry also needs to be considered. There can be differences in powder consumed during the process based on primitive (simple) geometry compared to complex surface geometry and dependent upon laser-on time (building versus positional movements).

The Pz parameter is compared with the Pa parameter and plotted as a function of layer height in Fig. 13. The coarse powder does not show a sensitivity to average or maximum texture profile based on layer height. The fine powder shows a more apparent trend with the lower layer height providing a lower average and maximum texture profile, although data does not match for all samples with other parameter variations.

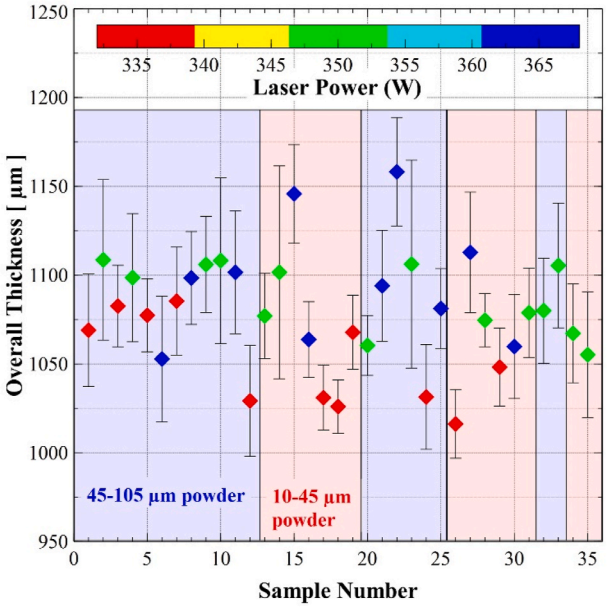

Fig. 12. Sample cross-sectional thickness compared to powder PSD and laser power.

The vertical orientation along the direction of the build was the primary interest for surface texture, but horizontal profile texture was also evaluated to evaluate differences. This is shown in Fig. 14. The line on the graph is provided as a reference assuming an arbitrary slope of 1. The coarse powder PSD indicates little difference (1%) between the vertical and horizontal directions. The fine powder profile is biased toward the vertical direction with a difference of 9%.

4. Discussion

The finer powder has more instances of subsurface particles than the coarse particles observed in the micrographs, because of the propensity for rapid solidification during the build (Anderson et al., 2018). This does not impact the surface texture and the finer powder still provides

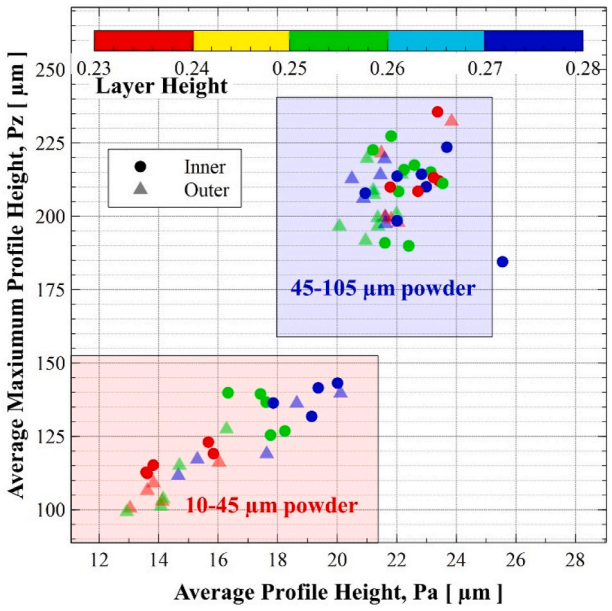

Fig. 13. Comparison of average profile height (Pa) to average maximum profile height (Pz).

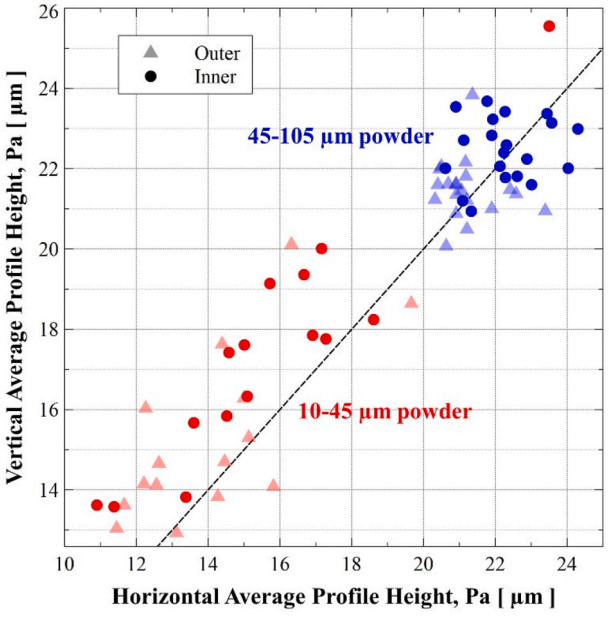

Fig. 14. Comparison of vertical and horizontal average profile height, Pa.

lower values overall. While literature reports that the finer powder tends to have flowability issues (Iams et al., 2021; Zhao et al., 2021), there were no issues observed with the 3-nozzle system used in this study. The fine powder samples indicate that the inner surface is predominately peaks while the outer surface is mostly valleys. The high degree of peaks for the inner surface indicates that powder particles are adhering to the surface as the NASA HR-1 alloy starts to cool (ie. excess powder capture). Due to the reduced volume, the finer powder requires less thermal energy to melt (Spierings et al., 2011). The finer powder PSD combined with the higher likelihood of powder trapped and recirculating in the enclosed racetrack increases the excess powder capture to the inner surface. During deposition of the fine powder, it was observed that powder was suspended in the build chamber, which was likely the lower end of the fine PSD (less than 25 to 30 µm). The higher velocity of the fine powder in the gas stream is ejected from the nozzle and causes rebounds off solidified surfaces (Gao et al., 2022). The coarse particles were shown to be more likely to break through the surface tension of the melt pool and likely to be melted or partially solidified (Singh et al., 2020).

While the Sa had a tighter range for the coarse powder than the fine powder, the opposite was true when evaluating with the Sz parameter (Fig. 8B). This indicates a higher range in the peaks and valleys with the coarse powder, which follows the visual observations of the full adherence or partial melting of the coarse powder overcoming the surface tension. There are limited instances of unmelted coarse powder observed subsurface. The coarse powder samples are dominated by the peaks for the inner and outer surface with the solidified material forming a tangential radius between the partially melted particles. The fine powder has a high concentration of unmelted particles across the surface and subsurface. The fine powder shows an approximate split of peaks and valleys, although valleys shown to be marginally higher for most samples. The concentration of these unmelted particles make up these peaks and valleys bonded by solidified material (Fig. 7F).

Uniform and consistent roughness is a significant consideration in component design fabricated from LP-DED, but the material quality and process ability to meet geometric requirements consistently is equally important. These factors can include the material density and the wall thickness. The lower porosity with fine powder has been observed in studies in other alloys (Kakinuma et al., 2016; Takemura et al., 2019), which can also be related to the increase in efficiency for the finer powder (Vundru et al., 2021). Townsend et al. points out that surface conditions may act as a fundamental observation to more underlying material defects (Townsend et al., 2016). The results from the current study align with this observation in that the reduced surface texture also resulted in a material with lower levels of porosity, although no significant defects were noted in either set of samples with varying powder PSD. This alone does not indicate that mechanical and thermophysical properties will match intended requirements, and the properties need to be confirmed with testing.

A prior study by Jinoop et al. indicates 38% increases in wall thickness with 83% increase in power (Jinoop et al., 2020). Other studies also reference the increase of the wall thickness due to the larger melt pool observed with increased laser power (Wirth et al., 2018; Jinoop et al., 2019). Low laser power can generate lack of fusion and detrimental effects on surface roughness and mechanical behavior, so a proper balance is required (G.A. Barragan et al., 2021). The reduction of travel speed also leads to increased wall thickness (Segerstark et al., 2014). Fine powders allow for uniform flow in the deposition nozzle and promote a small melt pool from the laser (DebRoy et al., 2018). However, in this study there was not a significant difference observed in the wall thicknesses between the fine and coarse powder with the power changes observed. The NASA HR-1 alloy also has tendency to be more sluggish during the build and the melt pool does not tend to flow out compared to other alloys.

The mechanisms that produce surface texture in the vertical and horizontal directions differ for thin-walls. The vertical roughness is related to the bead geometry (width and height), layer height, and the adherence of unmelted (residual) and partially melted powder to the outmost surfaces. The horizontal roughness relates to the adherence of the residual and partially melted powder assuming measurements are made nearly parallel with the bead. The low difference between the vertical and horizontal surfaces from this study provides validation that the surface roughness is near uniform, and the anisotropy is coming from the waviness. The parameters selected in this study provide good dilution of the melt pool eliminating discontinuities between layers for an optimal processing window (Fathi et al., 2006; Shim et al., 2016).

The major contributor to roughness in this study is the powder PSD with fine powder providing lower areal roughness and directional profile texture. The surface roughness map for samples 32 (coarse powder) and 34 (fine powder) is shown in Fig. 15. The particles are bonded at

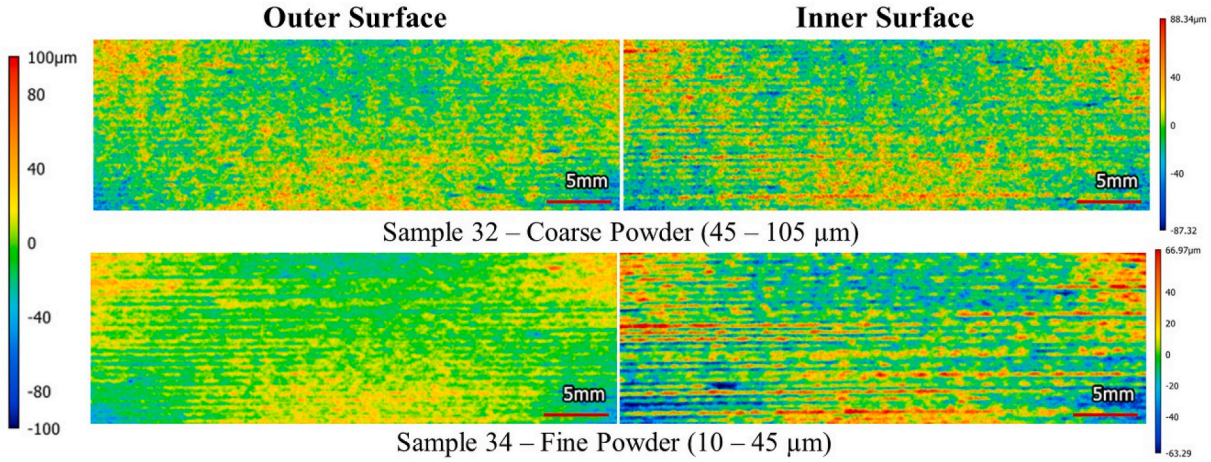

Fig. 15. Comparison of areal surface roughness map for coarse and fine powder, inner and outer surface.

various time periods during the solidification of the NASA HR-1 with some fully encapsulated with melted material and others partially bonded. The fine powder has a much higher sensitivity to the build parameters compared to the coarse powder when build parameters are changed. The volumetric heat capacity of the fine powder is 18% of the coarse powder and will tend to heat up quickly in the laser beam and become fully molten as it is injected into the melt pool (Pinkerton and Li, 2003).

The layer height did have a significant impact, albeit lower influence on surface texture. There was a higher degree of waviness present on the inner surface of the racetracks. Many prior studies showed the layering and obvious lateral menisci from LP-DED process. This was not readily apparent in the 1 mm thick NASA HR-1 samples, and waviness is not impacted by layer height. The directional surface roughness was within 9% for horizontal and vertical directions and considered uniform.

Based on the average, the inner surface has 1.67 µm higher roughness than the outer surface. This difference was also confirmed to be significant with a paired *t*-test for the mean at 0.01 significance level (99% confidence). This difference was also more pronounced in the fine powder sample (2.3 µm average) compared to the coarse powder (1.2 µm). It should be noted that there are four runs where the outer surface is higher than the inner surface. However, the differences were similar at 0.2–0.3 µm, while one sample was 1 µm, and all parameters were modified in unison. The commonality of these four runs is when layer height is set to the lowest (0.229 mm) or travel speed is set to the highest (800 mm/s).

Based on the DOE results and observed changes in parameters, the surface roughness can be reduced. The contour plots observing Sa as the factor are shown in Fig. 16. Similar plots were completed for vertical Ra showing nearly identical results. To reduce surface roughness to the lowest value for the NASA HR-1, the layer height should be set to the lowest values along with using the fine powder. The interaction of the other parameters only had minor contributions and did not impact results enough, so were maintained at nominal values. The fine powder and low layer height also provided low porosity material and desired wall thicknesses.

A practical balance of parameters should also be considered as results are used for part production. While surface roughness was reduced

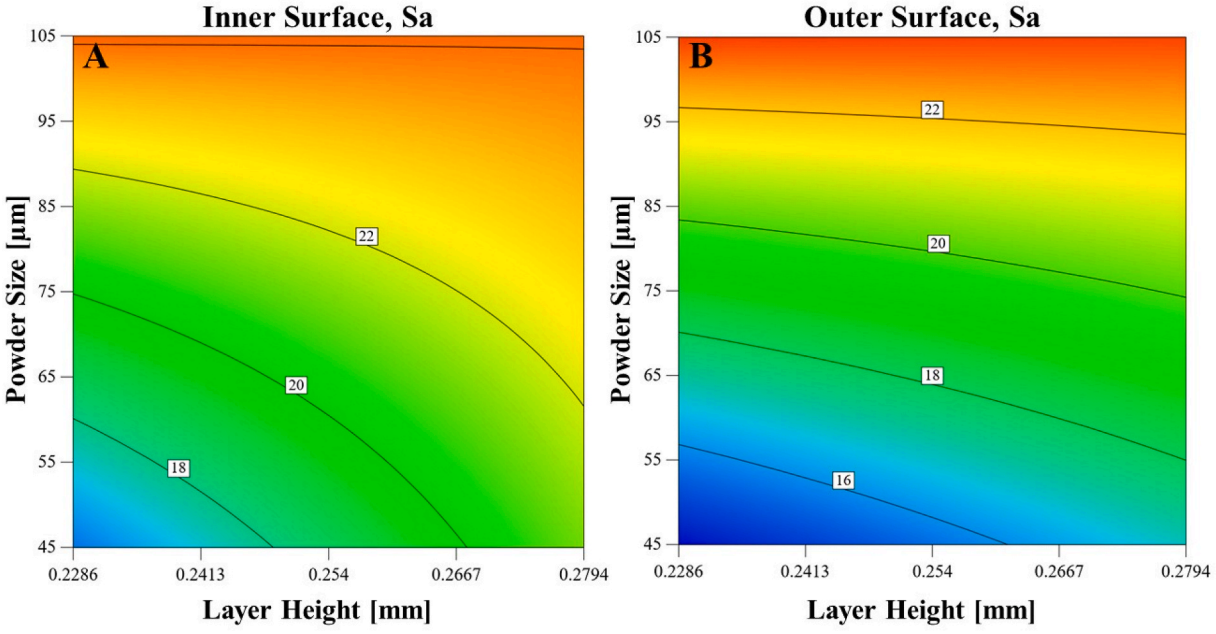

Fig. 16. Contour plot for average areal surface roughness with powder size and layer height interaction. The powder size is shown in maximum value (45 and 105 µm) and average areal roughness (Sa) units in µm.

with the lower layer height (0.229 mm) from the nominal (0.254 mm), the build time would increase. The roughness is increased from 15.6 μm at the lower layer height by 1 μm when the layer height is increased to 0.254 mm. This represents a 6% increase in average roughness (Sa), but a build time increase of 17%. The build time was calculated with a simple primitive geometry model changing the layer height, assuming a constant travel speed.

5. Conclusions

Industrialization of additively manufactured parts requires a detailed characterization of the microstructure and the resulting geometry such as wall thickness, defects such as porosity, and the surface texture for successful use in critical applications. In this study, closed racetrack NASA HR-1 alloy 1 mm thin-wall samples were built using the LP-DED process with rotary atomized fine and coarse powder to evaluate surface texture (roughness and waviness), basic geometry, and microstructure. These samples were successfully built using a single-bead deposition wall to a height of 25 mm. A design of experiments (DOE) was setup to evaluate the variation in parameters to determine the correlation and influence of the build parameters and powder particle size distribution (PSD). A total of 35 samples were successfully deposited with various parameters and were measured using a non-contact patterned light projection profilometer in the as-built condition. The samples were also evaluated using optical microscopy and scanning electron microscope (SEM) and sectioned to evaluate thickness, porosity, and roughness. The results were presented and summarized, and the following conclusions were drawn from the NASA HR-1 1 mm thin-wall samples.

- Surface roughness of LP-DED material is derived from excess or partially melted powder captured on the outmost surface of the trailing edge melt pool. The areal average surface roughness (Sa) is thus dominated by peaks of these particles.
- Partially or unmelted powder can be solidified in the subsurface and was observed to be a maximum of 2x the diameter of the powder PSD.
- Fine powder (10 to 45 μm) produces on average roughness 23% lower compared to the coarse powder (45 to 105 μm).
- The inner (enclosed) surface shows a higher average surface roughness, texture, and waviness compared to the outer surface due to ricochets, recirculation, and higher volume of powder available to bond to the surface during solidification. This is further exasperated with thin-wall depositions where powder efficiency is reduced and more powder available to bond to the outmost surface during solidification.
- The resulting surface roughness from the fine powder indicated a higher sensitivity to the parameter changes where the roughness with the coarse powder showed little change.
- The analysis of variance indicated that the powder, layer height, and interaction of these accounted for 90% of the inner surface roughness and 95% of the outer surface roughness.
- The fine powder produced samples with lower overall porosity and averaged 0.03% ± 0.01%, while the coarse samples had a higher range and averaged 0.13% ± 0.07%
- A wall thickness of 1.05 to 1.15 mm can be properly maintained with either coarse or fine powder and related to the laser power.
- Waviness was minimized using a lower laser powder (<363 W) and low layer height (<0.28 mm) to produce a uniform surface with minor waviness. The typically reported menisci of layering were not observed in the NASA HR-1 alloy thin-wall samples deposited with the optimized parameters and 3-nozzle configuration.
- Surface roughness can be minimized by using fine powder, laser power of 350 W, powder feedrate of 23 g/s, travel speed of 762 mm/s, and a low layer height of 0.229 mm. While the surface roughness is reduced at these parameters a balance should also be evaluated based on process economics. With the decreased layer height, the build time is increased by 17%. The layer height could be increased to 0.254 mm, and the impact on surface roughness would be a 6% increase (+1 μm).

The LP-DED process is maturing and was demonstrated to successfully deposit freeform thin-wall features. This process can provide an alternative to the laser powder bed fusion (L-PBF) process for large-scale parts that require thin-walls, such as heat exchangers with internal channels or flow passages. While AM has shown surface roughness higher than traditionally manufactured parts, this study showcases a detailed understanding of the surface textures. The understanding of surface texture is critical for increased or debits to flow performance in heat exchangers allowing enhanced heat transfer or increases in pressure drop. This study also demonstrated the repeatability of LP-DED thin-walls and a high-density deposition using the NASA HR-1 alloy for use in high-pressure hydrogen applications.

Author contributions

P.R.G. – Conceptualization, Methodology, Writing – Original Draft, Investigation, Resources; **A.C.** – Supervision, Review & Editing, Methodology; **E.G.** – Supervision, Review & Editing, Methodology.

B. Referee suggestions

Will be provided.

C. Crosscheck

No previous publications on this dataset exist.

Declaration of competing interest

The authors declare that they have no known competing financial interests or personal relationships that could have appeared to influence the work reported in this paper.

Acknowledgements

This research was funded by NASA under additive manufacturing development efforts through the Rapid Analysis and Manufacturing Propulsion Technology (RAMPT) project. This paper describes objective technical results and analysis. Any subjective views or opinions that might be expressed in the paper do not necessarily represent the views of the National Aeronautics and Space Administration (NASA) or the United States Government. The results from this study are solely for informational purposes and not an endorsement of any techniques by the authors, their employers, or the publishing journal.

Thank you to the following individuals that aided with discussions on experiments and data results: Ken Johnson (NASA retired), Agustin Diaz (REM Surface), RPM Innovations (RPMI), Tyler Blumenthal (RPMI), Sara Rengifo (NASA), Bhaskar Dutta (DM3D), Piero Colonna (TU Delft). The authors also acknowledge the use of DesignExpert and Veusz software.

References

Ahn, D.G., 2021. Directed energy deposition (DED) process: state of the art. Int. J. Precision Eng. Manufact. - Green Technol. Korean Soc. Precision Eng. 8, 703–742. https://doi.org/10.1007/s40684-020-00302-7.

Ahsan, M.N., 2011. Modeling and analysis of laser direct metal deposition of Ti-6Al-4V alloy. PhD Thesis, The University of Manchester 81–98.

Ahsan, M.N., Pinkerton, A.J., Moat, R.J., Shackleton, J., 2011. A comparative study of laser direct metal deposition characteristics using gas and plasma-atomized Ti–6Al–4V powders. Mater. Sci. Eng. 528, 7648–7657. https://doi.org/10.1016/j.msea.2011.06.074.

Alimardani, M., Fallah, V., Iravani-Tabrizipour, M., Khajepour, A., 2012. Surface finish in laser solid freeform fabrication of an AISI 303L stainless steel thin wall. J. Mater. Process. Technol. 212, 113–119. https://doi.org/10.1016/j.jmatprotec.2011.08.012.

American Society of Mechanical Engineers (ASME), 2019. Surface Texture : Surface Roughness, Waviness, and Lay : ASME B46.1-2019. New York, N.Y.

Anderson, I.E., White, E.M.H., Dehoff, R., 2018. Feedstock powder processing research needs for additive manufacturing development. Curr. Opin. Solid State Mater. Sci. 22, 8–15. https://doi.org/10.1016/j.cossms.2018.01.002.

Arrizubieta, J.I., Martínez, S., Lamikiz, A., Ukar, E., Arntz, K., Klocke, F., 2017. Instantaneous powder flux regulation system for Laser Metal Deposition. J. Manuf. Process. 29, 242–251. https://doi.org/10.1016/j.jmapro.2017.07.018.

Azarniya, A., Colera, X.G., Mirzaali, M.J., Sovizi, S., Bartolomeu, F., St Weglowski, M.k., Wits, W.W., Yap, C.Y., Ahn, J., Miranda, G., Silva, F.S., Madaah Hosseini, H.R., Ramakrishna, S., Zadpoor, A.A., St Weglowski, k M., Wits, W.W., Yap, C.Y., Ahn, J., Miranda, G., Silva, F.S., Madaah Hosseini, H.R., Ramakrishna, S., Zadpoor, A.A., 2019. Additive manufacturing of Ti–6Al–4V parts through laser metal deposition (LMD): process, microstructure, and mechanical properties. J. Alloys Compd. 804, 163–191. https://doi.org/10.1016/j.jallcom.2019.04.255.

Balichakra, M., Bontha, S., Krishna, P., Balla, V.K., 2019. Prediction and validation of residual stresses generated during laser metal deposition of γ titanium aluminide thin wall structures. Mater. Res. Express 6, 106550. https://doi.org/10.1088/2053-1591/ab38ee.

Balit, Y., Charkaluk, E., Constantinescu, A., 2020. Digital image correlation for microstructural analysis of deformation pattern in additively manufactured 316L thin walls. Addit. Manuf. 31, 100862 https://doi.org/10.1016/j.addma.2019.100862.

Barragan, G., Mariani, F., Coelho, R., 2021. Ti6Al4V thin walls production using laser directed energy deposition (L-DED) process. Int. J. Eng. Mater. Manufact. 6, 124–131. https://doi.org/10.26776/ijemm.06.03.2021.03.

Barragan, G.A., Rojas, D., Grass, J.S., Coelho, R.T., 2021. Observations on laser additive manufacturing (LAM) in terms of directed energy deposition (DED) with metal powder feedstock. Laser Eng. 50, 117–141.

Bhuvanesh Kumar, M., Sathiya, P., 2021. Methods and materials for additive manufacturing: a critical review on advancements and challenges. Thin-Walled Struct. 159, 107228 https://doi.org/10.1016/j.tws.2020.107228.

Bian, L., Thompson, S.M., Shamsaei, N., 2015. Mechanical properties and microstructural features of direct laser-deposited Ti-6Al-4V. J. Mater. (JOM) 67, 629–638. https://doi.org/10.1007/s11837-015-1308-9.

Bikas, H., Koutsoukos, S., Stavropoulos, P., 2019. A decision support method for evaluation and process selection of additive manufacturing. Procedia CIRP 81, 1107–1112. https://doi.org/10.1016/j.procir.2019.03.261.

Blakey-Milner, B., Gradl, P., Snedden, G., Brooks, M., Pitot, J., Lopez, E., Leary, M., Berto, F., du Plessis, A., 2021. Metal additive manufacturing in aerospace: a review. Mater. Des. 209, 110008 https://doi.org/10.1016/j.matdes.2021.110008.

Bold, M.-N., Zielinski, J., Ziegler, S., Johannes Henrich Schleifenbaum, 2020. Study of Laser Metal Deposition of IN718 on Inclined Planes: Influences of Inclination on Height and Width of Deposited Material. Metal Additive Manufacturing Conference. Orebro, Sweden.

Careri, F., Imbrogno, S., Umbrello, D., Attallah, M.M., Outeiro, J., Batista, A.C., 2021. Machining and heat treatment as post-processing strategies for Ni-superalloys structures fabricated using direct energy deposition. J. Manuf. Process. 61, 236–244. https://doi.org/10.1016/j.jmapro.2020.11.024.

Carroll, P.A., Pinkerton, A.J., Allen, J., Syed, W., Sezer, H.K., Brown, P., Ng, G.K.L., Scudamore, R., Li, L., 2006. The Effect of Powder Recycling in Direct Metal Laser Deposition on Powder and Manufactured Part Characteristics. Cost Effective Manufacture via Net-Shape Processing. Meeting Proceedings RTO-MP-AVT-139, Neuilly-sur-Seine, France, pp. 18-1–18-10.

Chen, P.-S., Mitchell, M., 2005. Aerospace Structural Metals Handbook ALLOY NASA-HR-1 Nickel Base Alloys-Ni. NASA. https://ntrs.nasa.gov/api/citations/20050182936/downloads/20050182936.pdf.

Chen, P.S., Katsarelis, C.C., Medders, W.M., Gradl, P.R., 2021. Segregation Evolution and Diffusion of Titanium in Directed Energy Deposited. NASA. https://ntrs.nasa.gov/citations/20210013649.

DebRoy, T., Wei, H.L., Zuback, J.S., Mukherjee, T., Elmer, J.W., Milewski, J.O., Beese, A. M., Wilson-Heid, A., De, A., Zhang, W., 2018. Additive manufacturing of metallic components – process, structure and properties. Prog. Mater. Sci. 92, 112–224. https://doi.org/10.1016/j.pmatsci.2017.10.001.

Diaz, A., 2019. Surface texture characterization and optimization of metal additive manufacturing-produced components for aerospace applications. Additive Manufact. Aerospace Industry 341–374. https://doi.org/10.1016/B978-0-12-814062-8.00018-2.

Dutta, B., Jared, B., Babu, S., 2019. Science, Technology and Applications of Metals in Additive Manufacturing, first ed. Amsterdam Elsevier.

El Cheikh, H., Courant, B., Branchu, S., Huang, X., Hascot, J.Y., Guilln, R., 2012. Direct Laser Fabrication process with coaxial powder projection of 316L steel. Geometrical characteristics and microstructure characterization of wall structures. Opt Laser. Eng. 50, 1779–1784. https://doi.org/10.1016/j.optlaseng.2012.07.002.

Errico, V., Campanelli, S.L., Angelastro, A., Dassisti, M., Mazzarisi, M., Bonserio, C., 2021. Coaxial monitoring of aisi 316l thin walls fabricated by direct metal laser deposition. Materials 14, 1–17. https://doi.org/10.3390/ma14030673.

Fathi, A., Toyserkani, E., Khajepour, A., Durali, M., 2006. Prediction of melt pool depth and dilution in laser powder deposition. J. Phys. Appl. Phys. 39, 2613–2623. https://doi.org/10.1088/0022-3727/39/12/022.

Fox, J.C., Moylan, S.P., Lane, B.M., 2016. Effect of process parameters on the surface roughness of overhanging structures in laser powder bed fusion additive manufacturing. Procedia CIRP 45, 131–134. https://doi.org/10.1016/j.procir.2016.02.347.

Gamon, A., Arrieta, E., Gradl, P.R., Katsarelis, C., Murr, L.E., Wicker, R.B., Medina, F., 2021. Microstructure and hardness comparison of as-built Inconel 625 alloy following various additive manufacturing processes. Results in Materials 12. https://doi.org/10.1016/j.rinma.2021.100239.

Gao, X., Yao, X.X., Niu, F.Y., Zhang, Z., 2022. The influence of nozzle geometry on powder flow behaviors in directed energy deposition additive manufacturing. Adv. Powder Technol. 33, 103487 https://doi.org/10.1016/j.apt.2022.103487.

Gharbi, M., Peyre, P., Gorny, C., Carin, M., Morville, S., Le Masson, P., Carron, D., Fabbro, R., 2013. Influence of various process conditions on surface finishes induced by the direct metal deposition laser technique on a Ti-6Al-4V alloy. J. Mater. Process. Technol. 213, 791–800. https://doi.org/10.1016/j.jmatprotec.2012.11.015.

Gradl, P.R., Protz, C.S., 2020. Technology advancements for channel wall nozzle manufacturing in liquid rocket engines. Acta Astronaut. 174 https://doi.org/10.1016/j.actaastro.2020.04.067.

Gradl, P.R., Teasley, T.W., Protz, C.S., Katsarelis, C., Chen, P., 2021a. Process development and hot-fire testing of additively manufactured NASA HR-1 for liquid rocket engine applications. AIAA Propulsion Energy 2021, 1–23. https://doi.org/10.2514/6.2021-3236.

Gradl, P.R., Tinker, D.C., Ivester, J., Skinner, S.W., Teasley, T., Bili, J.L., 2021b. Geometric feature reproducibility for laser powder bed fusion (L-PBF) additive manufacturing with Inconel 718. Addit. Manuf. 47, 102305 https://doi.org/10.1016/j.addma.2021.102305.

Gradl R, P, Tinker C, D, Park, A, Mireles R, O, Garcia, M, Wilkerson, R, Mckinney, C, 2022. Robust Metal Additive Manufacturing Process Selection and Development for Aerospace Components. J. Mater. Eng. Perf. (JMEP). https://doi.org/10.1007/s11665-022-06850-0.

Hemmasian Ettefagh, A., Guo, S., Raush, J., 2020. Corrosion performance of additively manufactured stainless steel parts: a review. Addit. Manuf. 37, 101689 https://doi.org/10.1016/j.addma.2020.101689.

Iams, A.D., Gao, M.Z., Shetty, A., Palmer, T.A., 2021. Influence of particle size on powder rheology and effects on mass flow during directed energy deposition additive manufacturing. Powder Technol. 396, 316–326. https://doi.org/10.1016/j.powtec.2021.10.059.

Imbrogno, S., Alhuzaim, A., Attallah, M.M., 2021. Influence of the laser source pulsing frequency on the direct laser deposited Inconel 718 thin walls. J. Alloys Compd. 856, 158095 https://doi.org/10.1016/j.jallcom.2020.158095.

Jafari, D., Wits, W.W., 2018. The utilization of selective laser melting technology on heat transfer devices for thermal energy conversion applications: a review. Renew. Sustain. Energy Rev. 91, 420–442. https://doi.org/10.1016/j.rser.2018.03.109.

Jamshidinia, M., Kovacevic, R., 2015. The influence of heat accumulation on the surface roughness in powder-bed additive manufacturing. Surf. Topogr. Metrol. Prop. 3 https://doi.org/10.1088/2051-672X/3/1/014003.

Jardin, R., Tuninetti, V., Tchuindjang, J., Hashemi, N., Carrus, R., Mertens, A., Duch, L., Tran, H.S., Habraken, A.M., 2020. Sensitivity analysis in the modelling of a high speed steel thin-wall produced by directed energy deposition. Metals 10, 1554.

Jardon, Z., Ertveldt, J., Hinderdael, M., Guillaume, P., 2021. Process parameter study for enhancement of directed energy deposition powder efficiency based on single-track geometry evaluation Process parameter study for enhancement of directed energy deposition powder efficiency based on single-track geometry evalua. J. Laser Appl., 042023 https://doi.org/10.2351/7.0000516.

Jinoop, A.N., Nayak, S.K., Yadav, S., Paul, C.P., Singh, R., Kumar, J.G., Bindra, K.S., 2021. Effect of scan pattern on Hastelloy-X wall structures built by laser-directed energy deposition-based additive manufacturing. J. Micromanufact., 251659842110363 https://doi.org/10.1177/25165984211036312.

Jinoop, A.N., Paul, C.P., Bindra, K.S., 2019. Laser-assisted directed energy deposition of nickel super alloys: a review. Proc. IME J. Mater. Des. Appl. 233, 2376–2400. https://doi.org/10.1177/1464420719852658.

Jinoop, A.N., Paul, C.P., Denny, J., Nayak, S.K., Krishna, V., Bindra, K.S., 2020. Laser additive manufacturing (LAM) of Hastelloy-X thin walls using directed energy deposition (DED): parametric investigation and multi-objective analysis. Laser Eng. 46, 15–34.

Jones, A., Leary, M., Bateman, S., Easton, M., 2021. Effect of surface geometry on laser powder bed fusion defects. J. Mater. Process. Technol. 296, 117179 https://doi.org/10.1016/j.jmatprotec.2021.117179.

Kakinuma, Y., Mori, M., Oda, Y., Mori, T., Kashihara, M., Hansel, A., Fujishima, M., 2016. Influence of metal powder characteristics on product quality with directed energy deposition of Inconel 625. CIRP Annals 65, 209–212. https://doi.org/10.1016/J.CIRP.2016.04.058.

Kalami, H., Urbanic, J., 2021a. Process planning solution strategies for fabrication of thin-wall domes using directed energy deposition. Int. J. Comput. Integrated Manuf. 1–17. https://doi.org/10.1080/0951192X.2021.1946851, 00.

Kalami, H., Urbanic, J., 2021b. Exploration of surface roughness measurement solutions for additive manufactured components built by multi-axis tool paths. Addit. Manuf. 38, 101822 https://doi.org/10.1016/j.addma.2020.101822.

Kasperovich, G., Becker, R., Artzt, K., Barriobero-Vila, P., Requena, G., Haubrich, J., 2021. The effect of build direction and geometric optimization in laser powder bed fusion of Inconel 718 structures with internal channels. Mater. Des., 109858 https://doi.org/10.1016/j.matdes.2021.109858.

Katsarelis, C., Chen, P., Gradl, P.R., Protz, C., Jones, Z., Marshall, N., Flight, S., Ellis, D., Evans, L., 2019. Additive manufacturing of NASA HR-1 material for liquid rocket engine component applications. In: JANNAF Joint Propulsion Conference. https://ntrs.nasa.gov/search.jsp?R=20200001007.

Kerstens, F., Cervone, A., Gradl, P., 2021. End to end process evaluation for additively manufactured liquid rocket engine thrust chambers. Acta Astronaut. 182, 454–465. https://doi.org/10.1016/j.actaastro.2021.02.034.

Khan, H.M., Karabulut, Y., Kitay, O., Kaynak, Y., Jawahir, I.S., 2020. Influence of the post-processing operations on surface integrity of metal components produced by laser powder bed fusion additive manufacturing: a review. Mach. Sci. Technol. 25, 118–176. https://doi.org/10.1080/10910344.2020.1855649.

Kim, M.J., Saldana, C., 2020. Thin wall deposition of IN625 using directed energy deposition. J. Manuf. Process. 56, 1366–1373. https://doi.org/10.1016/j.jmapro.2020.04.032.

Kladovasilakis, N., Charalampous, P., Kostavelis, I., Tzetzis, D., Tzovaras, D., 2021. Impact of metal additive manufacturing parameters on the powder bed fusion and direct energy deposition processes: a comprehensive review. Progress Add. Manufact. 6, 349–365. https://doi.org/10.1007/s40964-021-00180-8.

Klein, E., Ling, J., Aute, V., Hwang, Y., Radermacher, R., 2018. A review of recent advances in additively manufactured heat exchangers. Int. Refrigerat. Air Conditioning Conferen. 1–10.

Kong, C.Y., Carroll, P.A., Brown, P., Scudamore, R.J., 2007. The effect of average powder particle size on deposition efficiency, deposit height and surface roughness in the direct metal laser deposition process. In: 14th International Conference on Joining of Materials. TWI Technology Centre, Helsingør, Denmark.

Kotadia, H.R., Gibbons, G., Das, A., Howes, P.D., 2021. A review of laser powder bed fusion additive manufacturing of aluminium alloys: microstructure and properties. Addit. Manuf. 46, 102155 https://doi.org/10.1016/j.addma.2021.102155.

Lehmann, T., Rose, D., Ranjbar, E., Ghasri-Khouzani, M., Tavakoli, M., Henein, H., Wolfe, T., Jawad Qureshi, A., 2021. Large-scale metal additive manufacturing: a holistic review of the state of the art and challenges. Int. Mater. Rev. 66 https://doi.org/10.1080/09506608.2021.1971427.

Li, C., Liu, Z.Y., Fang, X.Y., Guo, Y.B., 2018. Residual stress in metal additive manufacturing. Procedia CIRP 71, 348–353. https://doi.org/10.1016/J.PROCIR.2018.05.039.

Li, Y., Ma, J., 1997. Study on overlapping in the laser cladding process. Surf. Coating. Technol. 90, 1–5. https://doi.org/10.1016/S0257-8972(96)03022-8.

Lin, K., Yuan, L., Gu, D., 2019. Influence of laser parameters and complex structural features on the bio-inspired complex thin-wall structures fabricated by selective laser melting. J. Mater. Process. Technol. 267, 34–43. https://doi.org/10.1016/j.jmatprotec.2018.12.004.

Liu, J., Li, L., 2005. Effects of powder concentration distribution on fabrication of thin-wall parts in coaxial laser cladding. Opt Laser. Technol. 37, 287–292. https://doi.org/10.1016/j.optlastec.2004.04.009.

Liu, Z., He, B., Lyu, T., Zou, Y., 2021. A review on additive manufacturing of titanium alloys for aerospace applications: directed energy deposition and beyond Ti-6Al-4V. J. Mater. (JOM) 73, 1804–1818. https://doi.org/10.1007/s11837-021-04670-6.

Lu, L., Shi, T., Zhang, J., Mei, Y., Cheng, D., Fu, G., Yu, S., 2021. Research on surface finish of thin-wall parts by laser with coaxial inside-beam powder feeding. J. Laser Appl. 33, 022003 https://doi.org/10.2351/7.0000206.

Mahamood, R.M., Akinlabi, E.T., 2018. Effect of powder flow rate on surface finish in laser additive manufacturing process. IOP Conf. Ser. Mater. Sci. Eng. 391, 12005. https://doi.org/10.1088/1757-899x/391/1/012005.

Mahamood, R.M., Akinlabi, E.T., 2014. Effect of laser power on surface finish during laser metal deposition process. In: Proceedings of the World Congress on Engineering and Computer Sciences (WCECS) Vol II, pp. 965–969.

Margerit, P., Weisz-Patrault, D., Ravi-Chandar, K., Constantinescu, A., 2021. Tensile and ductile fracture properties of as-printed 316L stainless steel thin walls obtained by directed energy deposition. Addit. Manuf. 37, 101664 https://doi.org/10.1016/j.addma.2020.101664.

Mazzarisi, M., Campanelli, S.L., Angelastro, A., Dassisti, M., 2020. Phenomenological modelling of direct laser metal deposition for single tracks. Int. J. Adv. Manuf. Technol. 111, 1955–1970. https://doi.org/10.1007/s00170-020-06204-x.

Mianji, Z., Kholopov, A.A., Binkov, I.I., Kiani, A., 2021. Numerical simulation of thermal behavior and experimental investigation of thin walls during direct metal deposition of 316L stainless steel powder. In: Lasers in Manufacturing and Materials Processing. https://doi.org/10.1007/s40516-021-00155-1.

Montgomery, D.C., 2019. Design and Analysis of Experiments, tenth ed. Wiley.

Morville, S., Carin, M., Peyre, P., Gharbi, M., Carron, D., Le Masson, P., Fabbro, R., 2012. 2D longitudinal modeling of heat transfer and fluid flow during multilayered direct laser metal deposition process. J. Laser Appl. 24, 032008 https://doi.org/10.2351/1.4726445.

Ngo, T.D., Kashani, A., Imbalzano, G., Nguyen, K.T.Q., Hui, D., 2018. Additive manufacturing (3D printing): a review of materials, methods, applications and challenges. Compos. B Eng. 143, 172–196. https://doi.org/10.1016/j.compositesb.2018.02.012.

Niknam, S.A., Mortazavi, M., Li, D., 2021. Additively manufactured heat exchangers: a review on opportunities and challenges. Int. J. Adv. Manuf. Technol. 112, 601–618. https://doi.org/10.1007/s00170-020-06372-w.

Pinkerton, A.J., Li, L., 2003. Effects of powder geometry and composition in coaxial laser deposition of 316L steel for rapid prototyping. CIRP Annals 52, 181–184. https://doi.org/10.1016/S0007-8506(07)60560-5.

Prasad, H.S., Brueckner, F., Kaplan, A.F.H., 2019. Powder catchment in laser metal deposition. J. Laser Appl. 31, 022308 https://doi.org/10.2351/1.5096130.

Riede, M., Knoll, M., Wilsnack, C., Gruber, S., Cubillo, A.A., Melzer, C., Brandão, A., Pambaguian, L., Seidel, A., Lopez, E., Brueckner, F., Leyens, C., 2019. Material characterization of AISI 316L flexure pivot bearings fabricated by additive manufacturing. Materials 12. https://doi.org/10.3390/ma12152426.

Rosen, D., Kim, S., 2021. Design and manufacturing implications of additive manufacturing. J. Mater. Eng. Perform. 30, 6426–6438. https://doi.org/10.1007/s11665-021-06030-6.

Segerstark, A., Andersson, J., Svensson, L.E., 2014. Review of laser deposited superalloys using powder as an additive. In: 8th International Symposium on Superalloy 718 and Derivatives 2014 391–408. https://doi.org/10.1002/9781119016854.CH31.

Shah, K., Pinkerton, A.J., Salman, A., Li, L., 2010. Effects of melt pool variables and process parameters in laser direct metal deposition of aerospace alloys. Mater. Manuf. Process. 25, 1372–1380. https://doi.org/10.1080/10426914.2010.480999.

Shamsaei, N., Yadollahi, A., Bian, L., Thompson, S.M., 2015. An overview of Direct Laser Deposition for additive manufacturing; Part II: mechanical behavior, process parameter optimization and control. Addit. Manuf. 8, 12–35. https://doi.org/10.1016/j.addma.2015.07.002.

Shim, D.S., Baek, G.Y., Seo, J.S., Shin, G.Y., Kim, K.P., Lee, K.Y., 2016. Effect of layer thickness setting on deposition characteristics in direct energy deposition (DED) process. Opt Laser. Technol. 86, 69–78. https://doi.org/10.1016/j.optlastec.2016.07.001.

Singh, A., Kapil, S., Das, M., 2020. A comprehensive review of the methods and mechanisms for powder feedstock handling in directed energy deposition. Addit. Manuf. 35, 101388 https://doi.org/10.1016/J.ADDMA.2020.101388.

Snyder, J.C., Thole, K.A., 2020. Understanding laser powder bed fusion surface roughness. J. Manuf. Sci. Eng. 142 https://doi.org/10.1115/1.4046504.

Sobota, V.C., van de Kaa, G., Luomaranta, T., Martinsuo, M., Roland Ortt, J., 2021. Factors for metal additive manufacturing technology selection. J. Manuf. Technol. Manag. 32, 1741–1779. https://doi.org/10.1108/JMTM-12-2019-0448.

Sow, M.C., De Terris, T., Castelnau, O., Hamouche, Z., Coste, F., Fabbro, R., Peyre, P., 2020. Influence of beam diameter on laser powder bed fusion (L-PBF) process. Addit. Manuf. 36, 101532 https://doi.org/10.1016/J.ADDMA.2020.101532.

Spierings, A.B., Herres, N., Levy, G., 2011. Influence of the particle size distribution on surface quality and mechanical properties in AM steel parts. Rapid Prototyp. J. 17, 195–202. https://doi.org/10.1108/13552541111124770.

Stimpson, C.K., Snyder, J.C., Thole, K.A., Mongillo, D., 2016. Scaling roughness effects on pressure loss and heat transfer of additively manufactured channels. J. Turbomach. 139, 1–10. https://doi.org/10.1115/1.4034555.

Takemura, S., Koike, R., Kakinuma, Y., Sato, Y., Oda, Y., 2019. Design of powder nozzle for high resource efficiency in directed energy deposition based on computational fluid dynamics simulation. Int. J. Adv. Manuf. Technol. 105 (10 105), 4107–4121. https://doi.org/10.1007/S00170-019-03552-1, 2019.

Tan, H., Fan, W., Qian, Y., Chen, Y., Liu, S., Lin, X., 2020. Influence of inclined substrate on process characteristics of directed energy deposition. Opt Laser. Technol. 129, 106288 https://doi.org/10.1016/j.optlastec.2020.106288.

Thompson, S.M., Aspin, Z.S., Shamsaei, N., Elwany, A., Bian, L., 2015a. Additive manufacturing of heat exchangers: a case study on a multi-layered Ti–6Al–4V oscillating heat pipe. Addit. Manuf. 8, 163–174. https://doi.org/10.1016/j.addma.2015.09.003.

Thompson, S.M., Bian, L., Shamsaei, N., Yadollahi, A., 2015b. An overview of Direct Laser Deposition for additive manufacturing; Part I: transport phenomena, modeling and diagnostics. Addit. Manuf. 8, 36–62. https://doi.org/10.1016/j.addma.2015.07.001.

Townsend, A., Senin, N., Blunt, L., Leach, R.K., Taylor, J.S., 2016. Surface texture metrology for metal additive manufacturing: a review. Precis. Eng. 46, 34–47. https://doi.org/10.1016/j.precisioneng.2016.06.001.

Vafadar, A., Guzzomi, F., Rassau, A., Hayward, K., 2021. Advances in metal additive manufacturing: a review of common processes, industrial applications, and current challenges. Appl. Sci. 11, 1213. https://doi.org/10.3390/app11031213.

Vundru, C., Singh, R., Yan, W., Karagadde, S., 2021. A comprehensive analytical-computational model of laser directed energy deposition to predict deposition geometry and integrity for sustainable repair. Int. J. Mech. Sci. 211, 106790 https://doi.org/10.1016/j.ijmecsci.2021.106790.

Wang, A., Wang, Hongze, Wu, Y., Wang, Haowei, 2021. 3D printing of aluminum alloys using laser powder deposition: a review. Int. J. Adv. Manuf. Technol. 116 https://doi.org/10.1007/s00170-021-07440-5.

Wang, D., Wu, S., Bai, Y., Lin, H., Yang, Y., Song, C., 2017. Characteristics of typical geometrical features shaped by selective laser melting. J. Laser Appl. 29, 022007 https://doi.org/10.2351/1.4980164.

Wang, S., Zhu, L., Dun, Y., Yang, Z., Fuh, J.Y.H., Yan, W., 2021. Multi-physics modeling of direct energy deposition process of thin-walled structures: defect analysis. Comput. Mech. 67, 1229–1242. https://doi.org/10.1007/s00466-021-01992-9.

Wirth, F., Arpagaus, S., Wegener, K., 2018. Analysis of melt pool dynamics in laser cladding and direct metal deposition by automated high-speed camera image evaluation. Addit. Manuf. 21, 369–382. https://doi.org/10.1016/J.ADDMA.2018.03.025.

Wu, Z., Narra, S.P., Rollett, A., 2020. Exploring the fabrication limits of thin-wall structures in a laser powder bed fusion process. Int. J. Adv. Manuf. Technol. 110, 191–207. https://doi.org/10.1007/s00170-020-05827-4.

Xu, L., Chai, Z., Chen, H., Zhang, X., Xie, J., Chen, X., 2021. Tailoring Laves phase and mechanical properties of directed energy deposited Inconel 718 thin-wall via a gradient laser power method. Mater. Sci. Eng. 824, 141822 https://doi.org/10.1016/j.msea.2021.141822.

Xue, P., Zhu, L., Xu, P., Ren, Y., Xin, B., Wang, S., Yang, Z., Ning, J., Meng, G., Liu, Z., 2021. CrCoNi medium-entropy alloy thin-walled parts manufactured by laser metal deposition: microstructure evolution and mechanical anisotropy. Mater. Sci. Eng. 817, 141306 https://doi.org/10.1016/j.msea.2021.141306.

Yan, L., Cui, W., Newkirk, J.W., Liou, F., Thomas, E.E., Baker, A.H., Castle, J.B., 2020. Mechanical properties evaluation of a Ti-6Al-4V thin-wall structure produced by a hybrid manufacturing process. In: Solid Freeform Fabrication 2018: Proceedings of a

the 29th Annual International Solid Freeform Fabrication Symposium - an Additive Manufacturing Conference. SFF 2018 291–301.

Zekovic, S., Dwivedi, R., Kovacevic, R., 2007. Numerical simulation and experimental investigation of gas-powder flow from radially symmetrical nozzles in laser-based direct metal deposition. Int. J. Mach. Tool Manufact. 47, 112–123. https://doi.org/10.1016/j.ijmachtools.2006.02.004.

Zhang, J., Shi, S., Fu, G., Shi, J., Zhu, G., Cheng, D., 2019. Analysis on surface finish of thin-wall parts by laser metal deposition with annular beam. Opt Laser. Technol. 119, 105605 https://doi.org/10.1016/j.optlastec.2019.105605.

Zhang, X., Tiwari, R., Shooshtari, A.H., Ohadi, M.M., 2018. An additively manufactured metallic manifold-microchannel heat exchanger for high temperature applications. Appl. Therm. Eng. 143, 899–908. https://doi.org/10.1016/j.applthermaleng.2018.08.032.

Zhang, Y., Wu, L., Guo, X., Kane, S., Deng, Y., Jung, Y.-G., Lee, J.-H., Zhang, J., 2017. Additive manufacturing of metallic materials: a review. J. Mater. Eng. Perform. 27, 1–13. https://doi.org/10.1007/s11665-017-2747-y.

Zhao, T., Cai, W., Dahmen, M., Schaible, J., Hong, C., Gasser, A., Weisheit, A., Biermann, T., Kelbassa, I., Zhang, H., Gu, D., Schleifenbaum, J.H., 2018. Ageing response of an Al-Mg-Mn-Sc-Zr alloy processed by laser metal deposition in thin-wall structures. Vacuum 158, 121–125. https://doi.org/10.1016/j.vacuum.2018.09.052.

Zhao, Y., Cui, Y., Hasebe, Y., Bian, H., Yamanaka, K., Aoyagi, K., Hagisawa, T., Chiba, A., 2021. Controlling factors determining flowability of powders for additive manufacturing: a combined experimental and simulation study. Powder Technol. 393, 482–493. https://doi.org/10.1016/j.powtec.2021.08.006.

Zhu, G., Li, D., Zhang, A., Pi, G., Tang, Y., 2012. The influence of laser and powder defocusing characteristics on the surface quality in laser direct metal deposition. Opt Laser. Technol. 44, 349–356. https://doi.org/10.1016/j.optlastec.2011.07.013.